

Review

A Review on Cementitious Self-Healing and the Potential of Phase-Field Methods for Modeling Crack-Closing and Fracture Recovery

Sha Yang ¹, Fadi Aldakheel ^{2,*}, Antonio Caggiano ^{1,3,*}, Peter Wriggers ²
and Eddie Koenders ¹

¹ Institute of Construction and Building Materials, Technical University of Darmstadt, Franziska-Braun-Straße 3, 64287 Darmstadt, Germany; yang@wib.tu-darmstadt.de (S.Y.); koenders@wib.tu-darmstadt.de (E.K.)

² Institute of Continuum Mechanics, Leibniz Universitaet Hannover, An der Universitaet 1, 30823 Garbsen, Germany; wriggers@ikm.uni-hannover.de

³ CONICET and LMNI-FIUBA, Universidad de Buenos Aires, Buenos Aires C1127AAR, Argentina

* Correspondence: aldakheel@ikm.uni-hannover.de (F.A.); caggiano@wib.tu-darmstadt.de (A.C.)

Received: 26 October 2020; Accepted: 18 November 2020; Published: 21 November 2020



Abstract: Improving the durability and sustainability of concrete structures has been driving the enormous number of research papers on self-healing mechanisms that have been published in the past decades. The vast developments of computer science significantly contributed to this and enhanced the various possibilities numerical simulations can offer to predict the entire service life, with emphasis on crack development and cementitious self-healing. The aim of this paper is to review the currently available literature on numerical methods for cementitious self-healing and fracture development using Phase-Field (PF) methods. The PF method is a computational method that has been frequently used for modeling and predicting the evolution of meso- and microstructural morphology of cementitious materials. It uses a set of conservative and non-conservative field variables to describe the phase evolutions. Unlike traditional sharp interface models, these field variables are continuous in the interfacial region, which is typical for PF methods. The present study first summarizes the various principles of self-healing mechanisms for cementitious materials, followed by the application of PF methods for simulating microscopic phase transformations. Then, a review on the various PF approaches for precipitation reaction and fracture mechanisms is reported, where the final section addresses potential key issues that may be considered in future developments of self-healing models. This also includes unified, combined and coupled multi-field models, which allow a comprehensive simulation of self-healing processes in cementitious materials.

Keywords: self-healing; phase-field; cement-based systems; precipitation; reaction; fracture; transport

1. Introduction

Concrete is characterized by its high compressive strength, a wide availability of its raw materials, and simple production methods, which is the main reason that it became the most commonly used construction material in the world [1,2]. However, its low tensile strength is the main reason that various types of cracks can occur in a concrete element that may adversely affect its service life [3]. While under internal, external, or environmental load, open or closed micro- and/or meso cracks may develop inside a concrete element that may successively result in a loss of structural integrity [4]. Open surface cracks may also allow water or hazardous substances to enter and thereby severely impairing its durability [5,6]. Therefore, improving the durability of concrete structures, asks for a limitation or reduction of the number of cracks where self-healing strategies could be solution.

In the last decades, enormous efforts have already been done to develop various kinds of self-healing methods for cementitious systems [7–15]. Most comprehensive scientific report so far is the RILEM TC-221-SHC [16], that summarizes the current research progress and defines the difference between “autogenic” and “autonomic” self-healing methods, depending on whether crack closure happens due to either the material itself [17–20], or is triggered by means of engineered additions [13,14,21–30].

From a modeling point of view, the presently existing numerical approaches can be grouped according to the nature of their particular self-healing mechanism into (1) chemical reaction-based models [12,31–34], for predicting carbonation, hydration, polymerization and precipitation phenomena; (2) transport phenomena-based models [35,36], in which the phases affecting the healing processes are transported through the concrete pore-structure network; and (3) fracture-based models, smeared [37–46] and discrete [47–53] crack approaches for predicting strength recoveries of self-healing systems.

When considering the number and type of experiments required to study the performance of self-healing concrete, it turns out that optimizing self-healing mechanisms through extensive experimental studies is a very demanding task. However, this task becomes more doable when employing numerical simulation models. However, most existing models do not incorporate physically/chemically driven boundary movements for an accurate simulation of solid–liquid interfaces. To overcome these difficulties, phase-field (PF) methods have been proposed as a powerful tool for handling moving interfaces caused by phase transitions [54–56]. In conventional numerical models for phase transformations and microstructural evolutions, interfaces are considered to be infinitely sharp and have to be schematized explicitly [57–59]. It leads to incompatibilities that makes calculations very complex and difficult to implement in a computer program. Contrarily, PF methods are based on thermodynamic principles and assume a diffuse interface, which makes them suitable for solving complex morphological evolutionary processes. The evolution of the “field”, over time and space, is controlled by the nonlinear Cahn–Hilliard diffusion equation and its relaxation by the Allen–Cahn equation [60,61]. For concrete, a self-healing mechanism is physically almost similar to a dissolution and/or precipitation principle that evolves at the cracked surfaces. It makes a PF modeling approach very suitable for solving this type of moving interface problems at cracked surfaces, caused by phase transformations.

This article provides a review on existing models to simulate self-healing in cracked concrete, with emphasis on PF methods. After the introduction in Section 1, the currently available self-healing methods for concrete are reported in Section 2. In Section 3, the possibility of using PF methods for simulating self-healing in concrete is presented and discussed. Then, in Section 4, the basic equations of a PF method are presented. Next, in Sections 5 and 6 existing PF techniques for precipitation and fracture in concrete are reported, respectively. Finally, items that should be addressed in self-healing models along with future research priorities and a concluding discussion on the whole article is given in Section 7.

2. Self-Healing Mechanisms in Concrete

In general, self-healing processes in cement-based materials can be divided into two categories: (1) autogenous self-healing and (2) autonomous self-healing [9,62,63]. Autogenous self-healing involves only the original components of a concrete. These components may, due to their specific chemical compositions, promote crack healing under favorable environmental conditions, driven by chemical reactions or transitions [10,64,65]. However, autonomous self-healing processes can only take place with the help of healing additives, such as microcapsules that may contain healing agents like polymers or bacterial spores [14,66]. Autogenous healing mechanisms have a limited healing capacity, typically only being able to heal cracks of about 100–150 μm in width [67]. In contrast to this, autonomous mechanisms can easily heal cracks up to 300 μm and sometimes even more than 1 mm [67]. These self-healing mechanisms are described below in detail.

2.1. Autogenous Self-Healing

Autogenous self-healing has been extensively investigated in the last decades [9,10,65,68,69], mainly by using experimental techniques. Figure 1a shows three main categories: physical, chemical, and mechanical healing. The physical healing mechanism is the process where the crack surface inside a cement matrix absorbs water and causes volume expansion [70,71]. The chemical healing mechanism consists of two main reactions, namely, a further hydration of the still unhydrated cement clinker inside a concrete, generating additional Calcium Silicate Hydrates (C-S-Hs), and carbonation of the additionally formed portlandite [65,72–74]. Finally, mechanical healing mechanisms refers to the filling of a crack with fine cement particles, which appear in a crack by water transport or diffusion [72]. The chemical mechanism is the primary and most promising healing method for hardened concrete at a young age [16]. Due to the relatively high content of unhydrated cement particles in these concretes, continuing hydration will still be possible and may result in a healing of cracks [18,64]. At later ages after crack initiation, the formation and growth of calcium carbonate crystals (CaCO_3) becomes the main healing mechanism [75]. Figure 1b,c shows the main healing products and their chemical components.

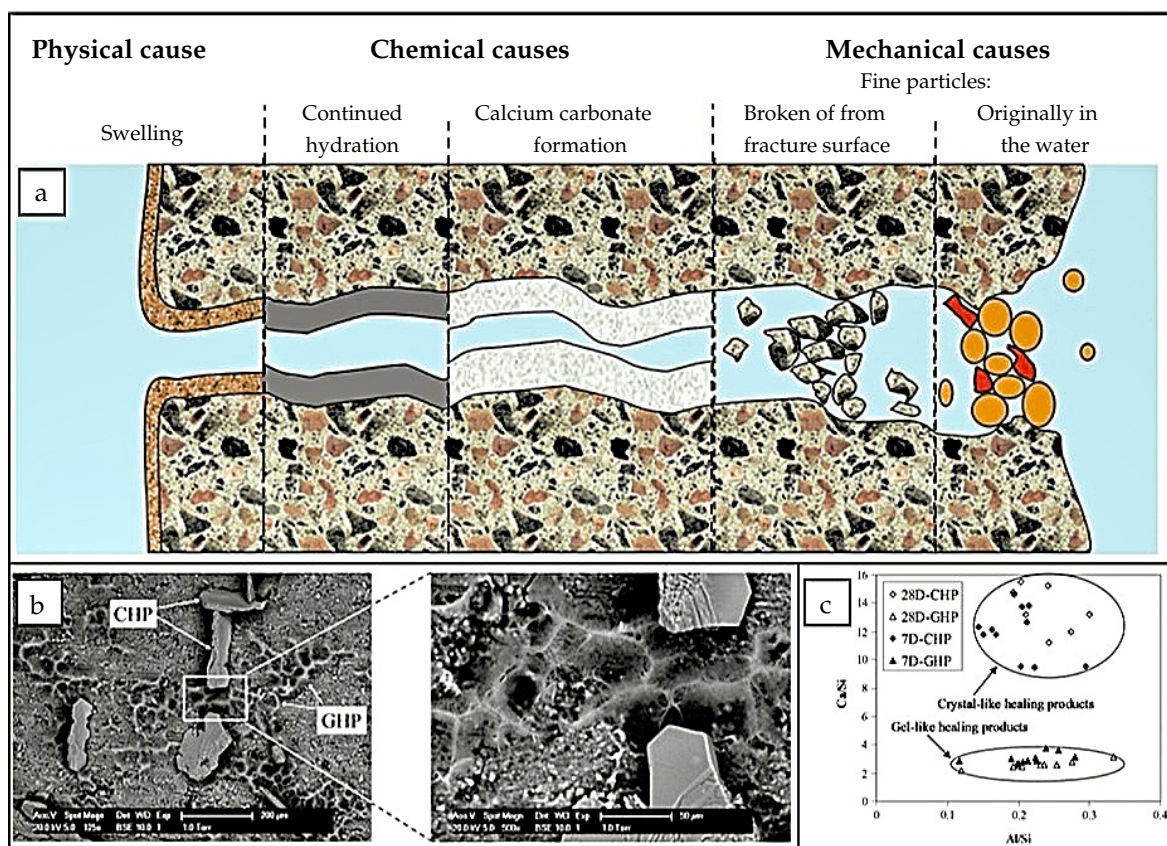


Figure 1. The autogenous self-healing mechanisms, products, and their corresponding chemical composition. (a) Schematic representation of the mechanisms of autogenic self-healing. Reproduced with permission from the authors of [70]. Copyright 2013, Springer. (b) Morphology of healing products (GHP refers to the gel-like healing product and CHP refers to the crystal-like healing product). Reproduced with permission from the authors [76]. Copyright 2013, Elsevier. (c) Ratios of Ca/Si and Al/Si of healing products with time. Reproduced with permission from the authors of [76]. Copyright 2013, Elsevier.

To improve the effectiveness of autogenous crack repair, an improved self-healing method called Dissoluble Encapsulated Particles (DEP) has been proposed [11,12,77]. In this self-healing method a certain amount of cement in a concrete mixture remains unhydrated for a predefined period of time

because of the pre-encapsulation of certain cement fractions which are covered with a thin membrane that can dissolve whenever it is affected by a crack (Figure 2). A crack in a cementitious surface may open the DEP membrane due to either (1) a dissolution mechanism caused by low pH-conditions, i.e., due to increased CO₂ ingress, or (2) by mechanical fracture. After this happened, the original unhydrated cement will be exposed to the local environmental temperature and humidity conditions causing the cement to react and finally close the crack [77].

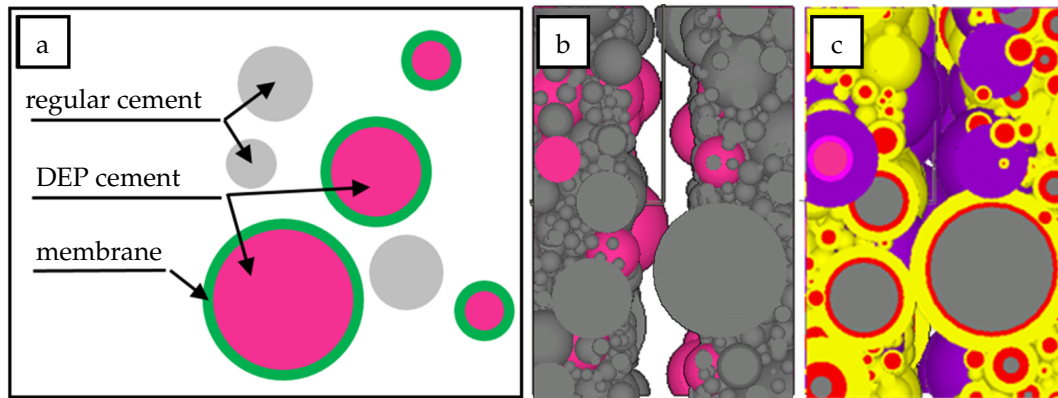


Figure 2. Self-healing with Dissoluble Encapsulated Particles (DEP): (a) Schematic representation of regular cement blended DEP cement [12]. (b) Initial state of microstructure by vol. –10% cement replacement by DEP [12]. (c) A high pH value will cause the DEP capsule to rupture, the healing agent will be released and a special hydration reaction with accompanying volume expansion will begin [77].

2.2. Autonomous Self-Healing

Autonomous self-healing is a method to improve the effectiveness of self-healing mechanisms for concrete, by either embedding encapsulated or non-encapsulated additions [62,67]. Until now, addition of encapsulated agents (micro/meso < 1 mm, macro ≥ 1 mm) is the most preferred method adopted for autonomous self-healing concrete [67], which may contain mineral [78,79], bacteria [14,28,80–88], and polymers [15,89,90]. Non-encapsulated additions may also contain these listed substances, but are added to a mixture in a pure, non-encapsulated, form where they become active directly after mixing of the concrete [91–93].

2.2.1. Self-Healing Based on Mineral Admixtures

Mineral admixtures are materials that are mixed in a concrete and react with water to form reaction products with an expanded volume to heal cracks developed in an already hardened concrete. With this healing mechanism [13,91,94,95], crack widths up to 120 μm can be repaired [67]. Depending on the type of mineral additives, three subcategories can be identified: (1) expansive additives, (2) geo-material based additives, and (3) chemical agents (crystalline additives) (Figure 3). Expansive additives develop reaction products with an increased volume that can fill the cracks [96]. Commonly used are sulfoaluminate based expansive additives (C-S-A) [78]. The geo-material-based additives consist of silicon dioxide, sodium aluminum silicate hydroxide, and bentonite clay, which have the capacity to swell [79,97,98]. When this type of geo-material is exposed to water, its volume may increase 15–18 times its initial dry volume [79]. The most basic crystalline additive is tricalcium silicate (C₃S), which is the main clinker component in cement and reacts with water to form calcium silicate hydrate C-S-H phases [26].

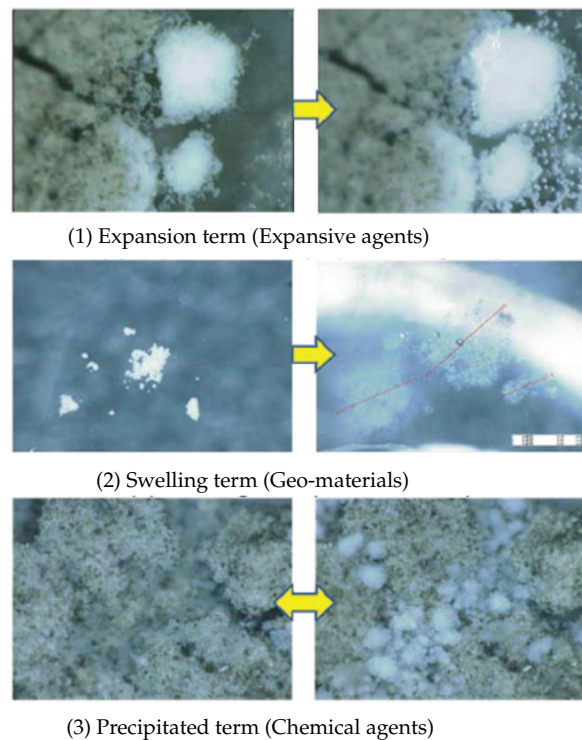


Figure 3. Three main self-healing mechanisms using mineral admixtures. Reproduced with permission from the authors of [79]. Copyright 2010, JCI.

2.2.2. Self-Healing Based on Bacteria

A certain category of bacteria can be applied for healing cracks in concrete [28]. It results in a closed crack which is watertight and has a limited capacity to restore the mechanical strength of a concrete [80–82]. The maximum crack width that can be healed with this system are $\sim 150 \mu\text{m}$ [83], which is rather limited whenever compared with other healing systems. Figure 4 shows a schematic impression of a fractured concrete with microencapsulated bacterial spores and the results of previous experiments [80,81,99].

Bacteria provide an important reaction component in a self-healing mechanism, where they are enhancing the calcium carbonate CaCO_3 production, needed for crack closing [100]. During healing, the mechanism passes the following two sequential steps; (1) conversion of calcium lactate and (2) hydrolysis of urea through (ureolytic) bacterial metabolism. In the first mechanism, oxygen and water penetrate into the concrete interior through cracks where the bacteria are activated to convert calcium lactate into CaCO_3 crystals and CO_2 . Portlandite particles near the cracks will further react with CO_2 to produce more CaCO_3 which precipitates at the crack surfaces [81]. In the second mechanism, many components capable of producing organic urea (e.g., *Bacillus cohnii*, *Sphaericus*, *Subtilis*, *Pasteurii*, *Megaterium*, and *Sporosarcina ureae*) can act as a catalyst during the self-healing process [101]. As it undergoes demineralization, negatively charged bacterial cells take up components from the cell wall and then react to CaCO_3 precipitates [102].

The efficiency of the precipitates generated by bacterial induction is determined first by the available water content and moisture movement in the concrete matrix [103,104], and second by the concentration of calcium ions, the pH of the pore solution, the concentration of inorganic carbon and by the presence of nucleation sites [105,106]. The first three are available in the concrete matrix, while the last one is related to the type of bacteria used [82]. In addition, factors that affect the effectiveness of healing include (1) the type of carrier (direct [107], encapsulated [108] containers like clay and aggregates [109,110]) and (2) the concrete compatible chemical reactions taking place in producing CaCO_3 [86,111].

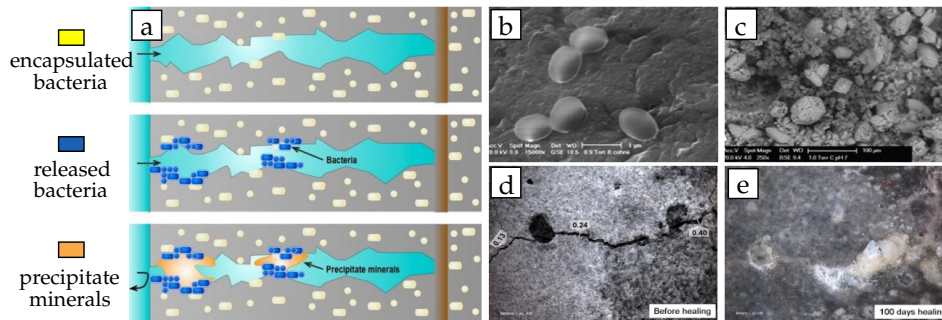


Figure 4. Self-healing mechanism using bacterial spores. (a) Schematic diagram of bacterial repair of concrete cracks. Bacteria on the surface of the crack are activated by water and precipitate minerals such as calcite to seal the crack and protect the reinforcement from external chemical attack. Reproduced with permission from the authors of [99]. Copyright 2018, Elsevier. (b) ESEM photomicrograph (15,000× magnification) of *B. cohnii* spores, showing that spore diameter sizes are up to 1 µm. Reproduced with permission from the authors of [80]. Copyright 2010, Elsevier. (c) Mineral precipitates (20–80 µm sized) on crack surfaces (250× magnification). Reproduced with permission from the authors of [80]. Copyright 2010, Elsevier. (d) Stereomicroscopic images of crack-healing process in bio-chemical agent-based specimen before and (e) after 100 days healing. Reproduced with permission from the authors of [81]. Copyright 2011, Elsevier.

2.2.3. Self-Healing Based on Adhesive Agents

This method is based on injecting adhesives into a crack to induce manual healing [112,113]. The crack widths which can be healed with these systems vary from 50 µm up to 250–300 µm [67,114]. Adhesive agents can be divided into one-component and multicomponent systems. Commonly used one-component adhesive agents are polyurethane [115] and epoxy [116]. Multicomponent adhesives are methylmethacrylate [117] and ureaformaldehyde/epoxy [113]. Adhesive agents are encapsulated in spherical capsules [112], tubular-shaped capsules [117,118], and hollow fibers [119–121] that are mixed with fresh concrete (Figure 5). When cracks occur, rupture of the encapsulation takes place, where the adhesive will be released into the crack by capillary action, initiating crack healing with time.

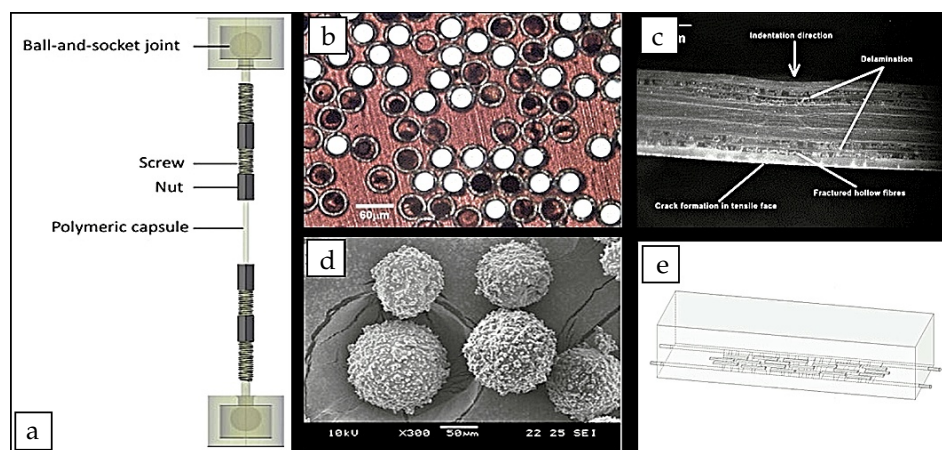


Figure 5. Self-healing mechanism based on adhesive agents. (a) Test setup used to determine the tensile strength of laboratory-scale hollow glass tubes with an outer hole of diameter 5 mm and an inner pin of diameter 3 mm. Reproduced with permission from the authors of [117]. Copyright 2015, Elsevier. (b) Hollow glass fibres of 60 µm external diameter with a hollowness of 50%. (c) Cross section through impact damaged hybrid solid glass/hollow glass/epoxy laminate. Reproduced with permission from the authors of [120]. Copyright 2005, Elsevier. (d) Spherical microcapsules with diameter of 120 ± 33 µm. Reproduced with permission from the authors of [122]. Copyright 2012, Elsevier. (e) Short glass/ceramic capsules attached to reinforcement, Reproduced with permission from the authors of [118]. Copyright 2015, Elsevier.

3. Phase-Field Methods for Modeling Concrete Self-Healing

The Phase Field (PF) method for simulating lower scale micro- and/or mesostructural cracking in materials has got an enormous upswing in the last decades. However, so far classical PF applications were focusing on the distribution of non-reactive multi-phase systems [123]; solidification problems [55,124]; solid-state phase changes [125,126]; grain growth, nucleation, and coalescence processes [127–129]; dislocation dynamics [130]; temperature inducing phase transformations [131]; liquid-phase sintering [132]; mass transport phenomena [133]; hydrodynamics [134]; and electromigration [135]. Recently, many problems in solid mechanics deal with the use of PF for describing fracture phenomena and to capture complex crack patterns [136–140]. Based on the present literature review, the following can be summarized.

- PF is an extremely powerful mathematical modeling scheme for accurately describing physical movements of phase boundaries.
- PF was mainly employed for solving solidification dynamics, material phase changes/separations, growing phases driven by chemo-kinetics and transport phenomena, nucleation and coalescence processes between particles in micro-to-mesostructures.
- PF has been successfully employed in fracture mechanics to capture the cracking response of brittle/ductile materials without the need for employing Discrete Crack Approaches (DCAs) and/or Smeared Crack Approaches (SCA).

Because of this, and as also supported by various state-of-the-art reports [55,56,141–144], PF models can be employed for self-healing of brittle or plastic (ductile) materials in a fundamental and consistent way. It will combine the impact of two main phase changes that occur simultaneously in a self-healing mechanism, i.e., chemical reactions and fracture. Gradual changes from the fully-cracked (failure) to the uncracked configuration can be driven through the so-called Phase-Field order parameter (ϕ). It will provide a smooth transition of all relevant phenomena between the fully cracked configuration and the intact material phases: this strength and crack recoveries actually represent the self-healing process. The governing equations of the proposed unified model will be derived in the framework of thermodynamics concepts, in terms of kinematics and balance equations, dissipation inequality and constitutive laws. Particularly, the free energy will be considered as the sum of the contributions due to elasticity, reaction PF and fracture PF. The free energy of the system is described in a unified form over the entire phase transition region. In this regard, the advantage of the PF method over other competitive numerical methods is its enormous capability of capturing movements of interfaces, without the need for introducing any additional ad hoc technique, criteria and/or remeshing strategies, and also without any explicit tracking of the actual interface positions of these coupled processes. The governing equations of PF models for chemical/moisture reactions and fracture processes, associated with self-healing, as well as the coupling among them, can be formulated in a unified PF framework. The next sections report a review on the available formulations for a unified and coupled set of PF approaches for modeling reactions and fracture of self-healing mechanisms in concrete.

4. Main Equations of a Phase-Field Approach

The phase-field (PF) approach is a very powerful technique to simulate complex physical phenomena in multi-field environments. The main attributions of this approach are simplicity and generality. A popular PF application is a diffusion interface model that is frequently used to simulate phase transformation problems in materials research [145–147]. The classical PF method is formulated based on the theory of Ginzburg and Landau, elaborated in the 1950s [148]. Compared with the sharp interface model, the PF diffusion interface model has the important advantage that no boundary conditions are specified on the interface between the different domains (Figure 6). A diffusive order parameter ϕ is a continuous function coordinate of time and space, which indicates each phase to convert between $0 \sim 1$ or $-1 \sim 1$ within a thin transition layer [54,144]. Moreover, ϕ is controlled by a

set of coupled partial differential equations that can be discretized and solved numerically by evolving the equations. Any phase transformation is driven by a reduction of the free energy of the system F , which can be described by a set of conserved c_i and non-conserved ϕ_i field variables. The domain of the model is the entire phase transition system. The free energy of the system consists of the energy contributions from the homogenous bulk phases F_{bulk} and the diffuse interface region F_{int} , according to [146]

$$F(\phi, c) = F_{bulk} + F_{int} = \int_V [f_{loc}(\phi, c) + f_{int}(\nabla\phi, \nabla c)] dV \quad (1)$$

where f_{loc} defines the local free energy density (including chemical, interfacial and elastic strain free energy density), while f_{int} defines the diffusive interface energy density.

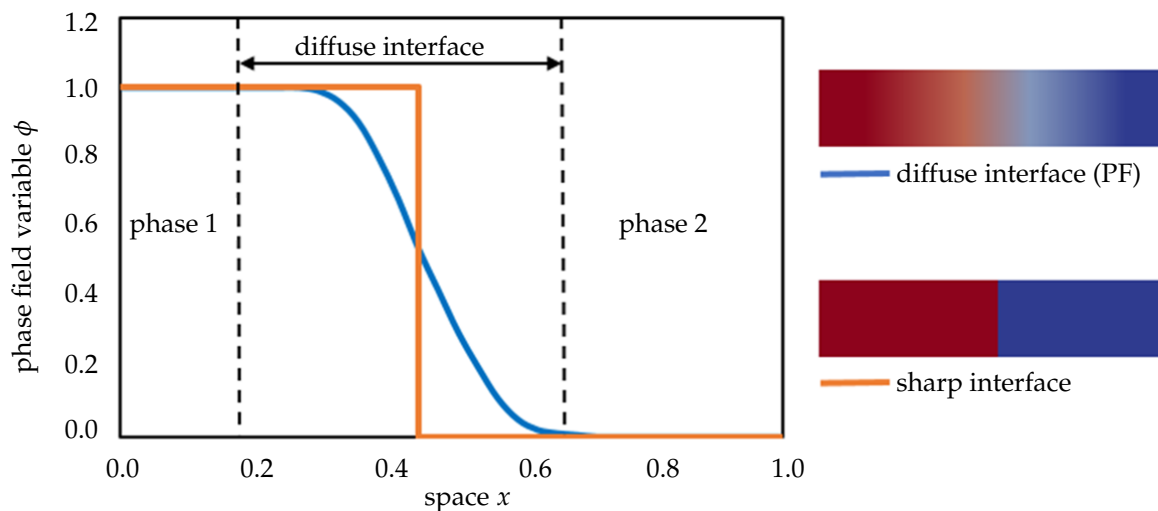


Figure 6. Schematic representation of sharp interface model and phase-field model.

From the computational point of view, monolithic or staggered algorithms can be computed to solve the problem unknowns, in which mechanical, chemical, interface, and phase-field variables are computed simultaneously or sequentially, respectively. For more details the interested reader is referred to the works in [136,149,150]. In those works, robust and efficient monolithic schemes were employed for the numerical implementation.

4.1. Evolution Equation

The generalized PF method is represented by the Ginzburg–Landau or Onsager kinetic equation combined with the well fitted Landau– or Redlich–Kister-type free energy density functionals, which are dependent on both conserved and non-conserved field variables [146]. The time-dependent evolution of the conserved field variables (chemical concentration) is defined using a modified Cahn–Hilliard equation [151], while the Allen–Cahn equation describes the transformations with non-conserved variables (e.g., crystal orientation, long-range order, crystal structure, and elastic strain) [152].

The Cahn–Hilliard equation is

$$\frac{\partial c_i(r, t)}{\partial t} = \nabla \cdot M_c \nabla \frac{\delta F}{\delta c_i(r, t)} \quad (2)$$

where c_i is the conserved concentration field variable, M_c is the kinetic coefficient of diffusion (associated mobility), t is the time and r is the spatial coordinate, ∇ is a vector of partial derivative operator, and δ denotes the variational derivation of the functional F .

The Allen–Cahn equation is

$$\frac{\partial \phi_i(r, t)}{\partial t} = -L_\phi \frac{\delta F}{\delta \phi_i(r, t)} \tag{3}$$

where $\phi_i(r, t)$ are the i different structure field variables with $i = 1, 2 \dots, n$, while L_ϕ is the kinetic structure operators (order parameter mobility). Depending on the problem, L_ϕ has different expressions [124,153,154].

4.2. Local Free Energy Function

The local free energy function is a key component in the PF model [155]. This function describes the free energy density of each bulk phase, whose coefficients are obtained from thermodynamic data [153]. The expression of the local free energy depends on the problem of interest. For example, a double-well form is often used for solidification [147,156]. When dealing with an electromigration problem, a double-obstacle potential is usually applied [55,157]. A crystalline energy function is used to describe an overlapped dislocation of an elastically anisotropic crystal [158–160]. When the problem is temperature-controlled, as in the melting and solidification processes of crystals, the local free energy function contains a temperature field [161,162]. In such cases, the phase-field is needed to be coupled with a temperature field [161–165]. Furthermore, a Landau-type polynomial potential can be applied for the treatment of a solid-state phase transformation [166–171]. Table 1 summarizes examples of the universal expressions, the graphs of the local free energies and existing phase-field applications.

Table 1. Expressions, graphs, and applications of the local free energy.

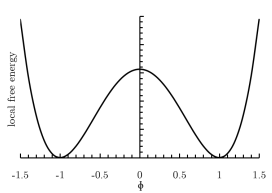
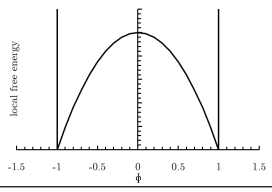
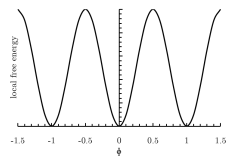
Double-well $f(\phi) = A \left(-\frac{1}{2}\phi^2 + \frac{1}{4}\phi^4 \right); \phi \in (-1, 1)$		
where A is the height of the potential energy between the two states at the minimum free energy.		
solidification coarsening and grain growth dislocation dynamics crack propagation crystal growth under stress biological application phase transformations in thin films electrochemical process	[54,55,147,154,156,172–180] [127,128,181–183] [184,185] [136–140] [186,187] [188,189] [190] [191–195]	
Double-obstacle $f(\phi) = \psi(\phi) + I_{[-1,1]}(\phi),$		
where, $\psi(\phi) = A(1 - \phi^2); I_{[-1,1]}(\phi) = \begin{cases} \infty & \phi > 1 \\ 0 & \phi \leq 1 \end{cases}$. when the phase transition only occurs in the narrow interface layer $\phi \in (-1, 1)$ instead of in regions outside the interfacial layer.		
solidification cell dynamical system stiffness maximization electromigration	[196,197] [198,199] [170] [200,201]	
Crystalline energy $f(\phi) = A \sin^2(\pi\phi); \phi \in (-\infty, +\infty),$		
where A is the energy barrier between two neighboring minima. This function is formulated with an infinite number of degenerated minima.		
dislocation system spiral growth	[158,159,202,203] [160,204]	

Table 1. Cont.

Potential with temperature field		
$f(\phi, T) = \frac{1}{8\alpha}(1 - \phi^2)^2 - (T_i - T_m)\phi$,		
where $T_i - T_m$ is the difference between the current temperature and the melting temperature; α is a positive constant.		
solidification	[161–165]	
Landau-polynomial		
$f(\phi) = f_{dis} + A\phi + B\phi^2 + C\phi^3 + D\phi^4 + E\phi^5 + F\phi^6$,		
where f_{dis} is the free energy of the disordered phase; $A \sim F$ are expansion coefficients related to temperature.		
solidification solid-state phase transformations electrochemical process crystal growth under stress phase transformations in thin films	[168,205–208] [166,167,209–211] [169,212] [170] [171,213,214]	

5. Phase-Field Modeling of Precipitation Reaction Mechanisms

Self-healing of concrete can be numerically treated as a precipitation process of solutes at the solid–liquid crack interface [215,216], which is time-dependent and controlled by chemical reactions and diffusion [36,217]. When the rate of the chemical reactions at the interface is sufficiently high and there is no fluid flow, diffusion will be the only mechanism left for solute transport. The whole process is then a diffusion-controlled precipitation one [216]. However, when the chemical kinetics is slow enough, the precipitation process becomes chemically determined [218]. A review of existing models for self-healing that are based on chemical reactions show that these models are employing a reaction-diffusion process to describe the self-healing evolution [12,31–34]. These models focus on two processes: (1) the diffusion mechanism where dissolved ions (e.g., calcium ions) are transferred from the concrete interior toward the surface of the crack, and (2) the precipitation of mineral ions reacting with, for example, carbon dioxide or carbonate ions to form calcium carbonate. They mostly consider how the chemical environment affects the formation of self-healing products and how to achieve agreement with experimental results [12,32–36,41,45,219].

However, these models have several limitations. First, they only simulate chemical reactions in solution and do not explicitly account for the change of the initial solid phase boundary due to the dissolution of soluble minerals at the fracture surface. Reaction diffusion models only include precipitation reactions in solution and do not simulate the dissolution reactions of the solid phase with a solution. Second, these models only uniformly simulate the healing process at the crack and do not accurately simulate the change in micro-morphology of the crack. The change in crack morphology is directly influenced by the concentration of aqueous substances and precipitations inside the solution [111]. In return, the change in crack morphology does affect the local concentrations of aqueous substances and precipitations in the solution. This interaction between the two factors is not reflected by existing models.

A PF method can fill these gaps. Figure 7 shows schematically a potential application of a PF model for an autogenous self-healing mechanism. The solid–liquid phase distribution is described by an eigenfunction in the value range [0, 1]. The solid phase can be subdivided into an initial solid phase (ϕ_1) and a healing solid phase (ϕ_2), while ϕ_3 represents the solution phase. The solid–solid (I_{SS}) and solid–liquid (I_{SL}) interfaces are simulated continuously. In addition to the solution (D_L), diffusion constants are distinguished between the concrete (D_{S1}) and the healing region (D_{S2}) due to differences in the meso- and microstructures. Neumann boundary conditions (Zero composition flux) were

for pure melt solidifications. Discontinuities in the solute concentration at the interface are explicitly considered. An additional term has been added to the solute diffusion equation to describe the discontinuity of the solute concentration gradient at the interface. In addition, a detailed asymptotic analysis was used to establish a connection between the sharp interface and the PF model by correlating the reaction rate parameter k with the microscopic PF parameters. This ensures that the PF model will converge to the corresponding sharp-interface limit. A modified solute diffusion equation is built up as follows,

$$\frac{\partial c}{\partial t} = D\nabla^2 c + A_1 \frac{\partial \phi}{\partial t} + A_2 \frac{\partial \phi / \partial t}{|\nabla \phi|} \left(D\nabla^2 \phi - \frac{\partial \phi}{\partial t} \right), \quad (4)$$

where the second additional term of the equation is corresponding to the discontinuity the solute concentration gradient at the interface. While the third additional term represents the net source or sink of the solute coming from the discontinuity in the solute concentration across the interface; D is the diffusion coefficient; A_1 and A_2 are two constants, which can be determined by the sharp-interface boundary conditions.

5.1.2. Noorden-Eck Model, 2011

Van Noorden and Eck [179] proposed a PF model for a precipitation and/or dissolution process. The model describes a single-phase free boundary problem with dynamic conditions at the moving boundary. The concentration on the precipitate side of the interface is specified, and the velocity normal to the interface is nonlinear dependent to the concentration on the other side of the interface. The evolution equation of ϕ and c is described according to

$$\frac{\partial \phi}{\partial t} = \frac{1}{\alpha} \Delta \phi - \frac{1}{\alpha \epsilon^2} p'(\phi) - \frac{1}{\alpha \epsilon} \beta k'(\phi) [f(c) + f'(c)(c - \rho)]; \quad (5)$$

$$\frac{\partial c}{\partial t} = D \nabla \left[\nabla c + (\rho - c) \frac{k'(\phi)}{k(\phi)} \nabla \phi \right], \quad (6)$$

where $p(\phi)$ is a double-well potential; $f(c)$ is a rate function; $k(\phi)$ is an interpolation function; α , β , D , and ρ are physical parameters; and ϵ is the thickness of an interfacial layer.

Redeker and Rohde [221,222] extended the Noorden–Eck model by incorporating curvature effects between two fluid phases to simulate precipitation in a porous medium. The model contains two immiscible fluids and one solid phase. Dissolved ions in one of the fluids can precipitate at the pore boundaries. Bringedal et al. [226] considered not only the diffusion of ions in the fluid phase, but also the effect of fluid flow on precipitation.

5.2. Metal Precipitation

Unlike solute precipitation, metal precipitation occurs in a supersaturated solid solution. Metals and metal oxides exist in the form of crystals. A crystal is a structure in which its atoms or molecules are arranged in an orderly fashion according to certain rules. A crystal is pure when all the components are just a single substance or a compound. If there is another substance involved that occupies the original atomic location and does not destroy the original structure, then this is a solid solution [233]. The original component is equivalent to a solvent and the foreign component is equivalent to a solute. As with a solution, when the solute in a solid solution is supersaturated in the solvent, it can no longer remain stable in the crystal structure and eventually precipitates [234].

The precipitate particles are generally metallic compounds, but may also be formed by aggregation of solute atoms in supersaturated solid solutions in a number of small solute-rich regions [235]. The precipitated particles act as barriers to dislocation movement, allowing significant increase in strength and hardness of most structural alloys of aluminum, magnesium, nickel, and titanium, as well as some steels and stainless steels [236]. The precipitation mechanisms of different binary and ternary alloys have been intensively studied by using PF models [182,237,238].

5.2.1. Wang–Chen Model, 1993

In the earlier study by Wang et al. [178], a PF model based on a microscopic kinetic model and elastic strain theory was developed to study the morphological evolution of the solid-state precipitation, controlled by transformation-induced elastic strain. The free energy of an inhomogeneous solid solution is given by the following equation,

$$F(c) = \frac{1}{2} \sum_{\phi'} W(r-r')c(r)c(r') + k_B T \sum_r [c(r) \ln c(r) + (1-c(r)) \ln(1-c(r))] \quad (7)$$

where $\phi(r, t)$ is the non-equilibrium single crystal sites of solute atoms, r is the crystal lattice site, $W(r-r')$ is the pairwise interaction energy of two atoms at the lattice site r and r' , and k_B is the Boltzmann's constant. The drawback of this model is that the matrix phase and the precipitates are iso-structurally treated. However, this assumption does not apply to the simulation of Al-Li alloy precipitation.

5.2.2. Rubin–Khachaturyan Model, 1999

Rubin and Khachaturyan [168] developed a 3D stochastic PF model for simulating the microstructural evolution of Ni-Al superalloys. This model considers the coherency strain in an elastic anisotropic system. The coarse grained stress-free free energy was expressed as

$$F = \int_V \left[\frac{1}{2} \left(\alpha_{ij} \nabla_{ic} \nabla_{jc} + \sum_{p=1}^3 \beta_{ij}(p) \nabla_{i\phi_p} \nabla_{j\phi_p} \right) + f(c, \phi_1, \phi_2, \phi_3) \right] d^3r \quad (8)$$

where α_{ij} and $\beta_{ij}(p)$ are the gradient coefficients, ∇_{ic} and ∇_{jc} denote the gradient terms of multi-composition profile $c(r, t)$, $\nabla_{i\phi_p}$ and $\nabla_{j\phi_p}$ are the gradient terms of multi-component long-range order parameter $\phi(r, t)$, the specific free energy $f(c, \phi_1, \phi_2, \phi_3)$ is approximated by a polynomial, and the second integral term is the total strain energy functional based on the Fourier transform microelasticity method.

5.2.3. Chen–Ma Model, 2004

Chen et al. [177] designed a quantitative PF modeling scheme for multicomponent diffusion-controlled precipitate growth and dissolution in Ti-Al-V system in which the thermodynamic and kinetic data of existing databases CALPHAD was directly inserted into the PF model. The total Gibbs free energy is described as follows,

$$G(T, c, \phi) = \frac{1}{V_m} \int_V \left[G_m(T, c_i, \phi) + \sum_{i=1}^{n-1} \frac{k_i}{2} |\nabla c_i|^2 + \frac{k_\phi}{2} |\nabla \phi|^2 \right] dV. \quad (9)$$

where G_m is the local molar Gibbs free energy; k_i and k_j are the gradient-energy coefficients for concentration and order parameter inhomogeneities, respectively; V_m is molar volume.

The temporal evolution of the composition is governed by Cahn–Hilliard diffusion equation on the basis of the phenomenological Fick–Onsager equations

$$\frac{1}{V_m^2} \frac{\partial c_k}{\partial t} = \nabla \cdot \sum_{j=1}^{n-1} M_{kj}(T, c_i, \phi) \nabla \frac{\delta G}{\delta c_i} \quad (10)$$

where M_{kj} are chemical mobilities related to atomic mobilities.

6. Phase-Field Modeling for Fracture Mechanisms

Fracture mechanics of concrete is a topic of intensive research during the last years. Simulation technology for analyzing crack initiation and propagation in concrete are numerous [58,239–255]. Besides boundary and finite element methods for linear elastic fracture analysis, different versions of the so called eXtended Finite Element Method (XFEM) are frequently applied [256,257].

Starting with the works of Bourdin et al. [258] and Miehe et al. [141], fracture processes were modeled explicitly by a PF approach. Due to its simplicity this methodology gained a wide interest and started to be used in the engineering community since 2010. From there on many scientist have worked in this field and developed PF approaches for finite elements methods (FEM), isogeometric analysis (IGA), and recently also for the virtual element methods (VEM). The main driving force for these developments is the possibility to handle complex fracture phenomena within numerical methods in various dimensions. Thus, research on PF approaches is still actual and points in many different directions.

In this review article, the simulation of fracture processes in concrete is achieved by utilizing the continuum PF method, which is based on the regularization of sharp crack discontinuities. This avoids the use of complex discretization methods for crack discontinuities and can account for multi-branched cracks within a solid skeleton (e.g., hydrated cement paste, unhydrated clinker particles, and stones). In particular due to the over-complicated geometry and content of concrete at multi-scales, in Figure 8 an example for PF modeling of water-induced failure mechanics in concrete microstructure is presented. In recent years, several brittle [259–296] and ductile [149,297–324] PF fracture formulations have been proposed in literature. These studies range from modeling 2D/3D small and large strain deformations, variational formulations, multi-scale/physics problems, mathematical analysis, different decompositions and discretization techniques with many applications in science and engineering. All these examples demonstrate the potential of PF method for crack propagation.

The aforementioned PF approaches consider the fracture behavior of concrete, i.e., as a crack initiation and propagation. However, an important aspect in concrete is the treatment of the crack-closure effects. This response was firstly investigated in the works [325,326] for fatigue crack closure under cyclic tension. Thereby, the results indicate a fatigue crack, propagating under zero-to-tension loading may be partially or completely closed at zero load. A review of this physical phenomena can be seen in [327–329]. To the author's best knowledge, a PF approach for modeling crack closure is still an open issue. To this end, cohesive elements along the crack path will be coupled with the PF formulations to prevent overlapping of the crack faces. Another future direction is to use a contact scheme at the crack faces similar to the work developed by [330]. A further important aspect is the PF modeling of crack-closure induced by a self-healing mechanism (introduced in Section 3) in cementitious systems. These topics await investigation.

6.1. Fundamental Variational Formulations

In Griffith-type fracture formulations, the mechanical deformation denoted generally by “state” and the sharp crack surface Γ in a brittle elastic solid (e.g., cement paste) are determined by the incremental minimization problem developed by Francfort and Marigo [331] as

$$E(\text{state}, \Gamma) = \int_{V \setminus \Gamma} f(\text{state}) \, dV + G_c \mathcal{H}(\Gamma) \rightarrow \text{Min!} \quad (11)$$

where G_c is the Griffith critical surface energy release and $\mathcal{H}(\Gamma)$ is the Hausdorff surface measure of the crack set Γ . In Equation (11), the functional E has a structure identical to that for image segmentation developed by Mumford and Shah [332]. It consists of the strain energy stored in the solid as well as the energy release due to fracture.

6.2. Regularized Variational Theory

The numerical evaluation of the sharp crack interface in the functional E (Equation (11)) is not suitable within a standard finite element framework, as outlined in the work of Bourdin et al. [258]. Therefore, a regularized crack interface using a specific regularization profile γ is introduced in the studies of Miehe et al. [141,297]. It is based on a geometric regularization of sharp crack discontinuities that is governed by a crack PF

$$\phi \in [0, 1] \quad \text{with} \quad \dot{\phi} \geq 0 \quad (12)$$

It characterizes locally for the initial condition $\phi = 0$ the unbroken and for $\phi = 1$ the fully broken state of the material. Thus, the critical fracture energy is approximated by

$$G_c \mathcal{H}(\Gamma) \approx \int_V G_c \gamma(\phi, \nabla\phi) dV \quad \text{with} \quad \gamma(\phi, \nabla\phi) := \frac{1}{2l_f} \phi^2 + \frac{l_f}{2} |\nabla\phi|^2 \quad (13)$$

in terms of the crack surface density function per unit volume of the solid. The regularization is governed by a fracture length scale l_f . Note that the limit for vanishing the fracture length scale $l_f \rightarrow 0$ gives the sharp crack surface Γ .

Therefore, the minimization problem represented by Equation (11) can be expressed in the following form,

$$\tilde{E}(\text{state}, \Gamma) = \int_V \widehat{W}(\text{state}, \phi, \nabla\phi) dV \rightarrow \text{Min!} \quad (14)$$

defined in terms of the total work density function \widehat{W} as

$$\widehat{W}(\text{state}, \phi, \nabla\phi) = g(\phi) f(\text{state}) + G_c \gamma(\phi, \nabla\phi), \quad (15)$$

contains a degraded elastic work density and the crack energy release per unit volume. $g(\phi)$ is a degradation function defined as $g(\phi) = (1 - \phi)^2$. It describes the degradation of the solid with the evolving crack phase-field ϕ , as depicted in Figure 8b–d.

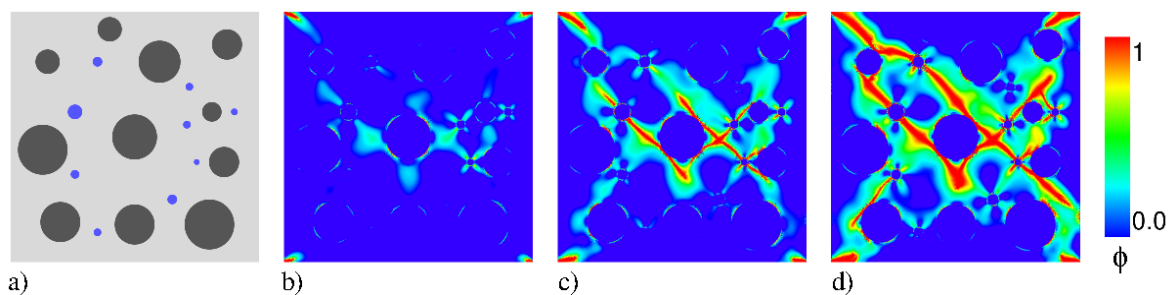


Figure 8. Concrete failure in poro-elasto-plastic media. (a) Schematic of the concrete idealized microstructure: Light gray color refers to the hydrated cement paste, dark gray color stands for the unhydrated clinker particles, and blue color depicts the water content. (b–d) Evolution of crack phase-field ϕ for different deformation states up to final failure, as outlined in [150].

7. Discussion and Conclusions

Based on the above literature review, it can be observed that PF methods have a great potential for simulating self-healing mechanisms in concrete. Therefore, it can be applied to solve problems that cannot be addressed by commonly applied models. It has the potential of an unprecedented breakthrough. As self-healing of concrete is a rather complex process, it is an interaction between physical, chemical and mechanical mechanisms. Obtaining a novel, versatile model for self-healing concrete is a multidisciplinary study involving civil engineering, materials science, and chemistry.

Many studies have been conducted in these fields using the PF approach, while it will be a great reference for the development of a self-healing PF model.

In future research, it would be recommended to include in the polynomial system of the PF approach the pore structure, concrete matrix, water dissolution, and hydration product phases at the crack front. In this way, the free-energy equations will combine hydration kinetics, crystallization kinetics, polymerization reaction kinetics, mass transport and chemical energies to provide a detailed description of the phase nucleation and growth mechanisms at the crack front. Coupling a reactive PF model with a fracture PF model allows to simulate the crack development and its mechanical self-healing recovery effects at different stages and under different environmental conditions. In order to achieve this goal, there are several self-healing mechanisms that need to be studied in great detail. Validating these models should be continuously done by comparing them with experimental results. The following potential future steps are identified:

1. Evolution of the pore structure at the crack surface:

During the process of autonomous self-healing, soluble substances at the crack surface enter the solution and undergo various dissolution reactions, followed by hydration and carbonation crystallization reactions. Part of the solution will diffuse into the capillary pores of the concrete matrix, where crystallization and precipitation also occur. The growth of the cracked surface also forms a new pore structure, which further affects the diffusion and chemical reaction processes. Thus, the pore structure of the crack boundary is constantly changing with ongoing reaction. Its interaction with the crack morphology, reactant concentration, and mass transport needs to be investigated in the future.

2. Influencing factors and simulations for mechanical repair of cracks:

The fracture PF part is a combination of elastic and fracture energies. Elastic free energy will follow the classical assumptions while the fracture part will account for the fracture toughness, order formulation, evolution equations, and healing regain laws. Moreover, both are closely related to the packing density field. This is because the mechanical properties at fracture mainly depend on the solid-phase continuity. The mechanical properties are enhanced in a homogeneously dense position of the filler and, conversely, worse in the disconnected parts of the solid phase. The packing density field, in turn, is related to the mass transport. Therefore, a numerical transport–mechanical coupling strategy shall be developed to simulate the overall performance of the self-healing mechanism.

3. Evolution of crack healing morphology:

The morphology of the crack greatly influences its local healing effect. At the crack tip, healing products are produced faster and more frequently because of the higher concentration of reactants. The movement of the crack tip is faster than at other locations. Thus the crack morphology changes continuously with the healing process. As the PF model avoids tracking the boundary conditions at the interface and instead simulates the evolution of the auxiliary field. Therefore, the evolution of the interfacial morphology is easier to simulate. In addition, the simulation of interfacial morphology will take into account the distribution of bacteria, adhesive agents and mineral admixtures. Therefore, the macroscopic representation of a crack healing morphology shall be simulated from a micro-level point of view.

4. Free energy to distinguish between various product phases:

Self-healing products contain multiple substances (CSH, CH, or additional byproducts) that, although they have the same healing mechanism (aggregation, crystallization and precipitation), their chemical reaction kinetics are different. This affects the rate of healing of the cracks as a whole. Therefore, the free energies of the various product phases and the corresponding thermodynamic parameters will be distinguished in the future and reflected in specific simulations.

5. Determination of PF parameters:

A formulation for the determination of the PF parameters needs to be provided. Information on the PF parameters and their interrelationships will be obtained from thermodynamic and diffusion databases in combination with experimental data. Combined with the second law of thermodynamics and non-equilibrium thermodynamics, the self-diffusion, mutual diffusion, and chemical diffusion coefficients will be related to the diffusion mobility (M). The order parameter mobility (L) will be derived and their relationship to other phase-field parameters will be investigated.

6. Development of a three-dimensional model:

As a self-healing process includes complex physical-chemical-mechanical processes, these mechanisms can only be accurately simulated in a fully three-dimensional system. Therefore, a three-dimensional simulation of the self-healing process need to be performed with realistic boundary conditions. The simulation results need to be verified and compared with 3D computed tomography scan (CT scan) results of concrete specimens.

In conclusion, the use of a PF method is feasible and has a significant application advantages in the field of self-healing concrete applications. Although this method still has a long way to go before it becomes a fully fledged simulation tool, these early studies are considered to be an important step towards reaching this goal.

Author Contributions: Conceptualization, S.Y. and A.C.; data curation, S.Y., F.A., A.C.; writing—original draft preparation, S.Y.; writing—review and editing, everybody; supervision, A.C and F.A.; project administration, E.K., P.W.; funding acquisition, E.K. All authors have read and agreed to the published version of the manuscript.

Funding: This research was funded by National German DFG organization: (i) under project number 387065993 titled “Form filling ability of fresh concrete: A time and hydration dependent approach”, as part of DFG SPP 2005 program “Opus Fluidum Futurum—Rheology of reactive, multiscale, multiphase construction materials”; and (ii) under project number 426807554 titled “Experimentally supported multi-scale Reactive Transport modeling of cementitious materials under Acid attack (ExpeRTa)”.

Acknowledgments: The authors in TU Darmstadt acknowledge the support by the German Research Foundation (DFG) under project number 353981539 titled “Visualisierung und mikromechanische Modellierung der Gefügeänderung von zyklisch beanspruchten Hochleistungsbetonen unter besonderer Berücksichtigung hygrischer und thermischer Randbedingungen”, as part of DFG SPP 2020 program “Zyklische Schädigungsprozesse in Hochleistungsbetonen im Experimental-Virtual-Lab”. In addition, the authors would like to thank the EU-funded project “CA15202—Self-healing As preventive Repair of COncrete Structures”. The authors in LUH gratefully acknowledges support for this research by the German Research Foundation (DFG) in the Priority Program SPP 2020 within the project WR 19/58-2 titled “Wasserinduzierte Schädigungsmechanismen zyklisch beanspruchter Hochleistungsbetone”.

Conflicts of Interest: The authors declare no conflicts of interest.

References

- Shetty, M. *Concrete Technology*, S; Chand and Company Ltd.: New Delhi, India, 2005.
- Perlovsky, L.I. Conundrum of combinatorial complexity. *IEEE Trans. Pattern Anal. Mach. Intell.* **1998**, *20*, 666–670. [[CrossRef](#)]
- Kaplan, M. Crack propagation and the fracture of concrete. *J. Proc.* **1961**, *58*, 591–610.
- Frosch, R.J. Another look at cracking and crack control in reinforced concrete. *Struct. J.* **1999**, *96*, 437–442.
- Hillerborg, A.; Mod er, M.; Petersson, P.E. Analysis of crack formation and crack growth in concrete by means of fracture mechanics and finite elements. *Cem. Concr. Res.* **1976**, *6*, 773–781. [[CrossRef](#)]
- Roumaldi, J.; Batson, G.B. Mechanics of Crack Arrest in Concrete. *J. Eng. Mech. Div. ASCE Proc.* **1963**, *89*, 147–168.
- Ferrara, L.; Asensio, E.C.; Monte, F.L.; Flores, M.R.; Moreno, M.S.; Snoeck, D.; Mullem, T.V.; Belie, N.D. Experimental characterization of the self-healing capacity of cement based materials: An overview. *Proceedings* **2018**, *2*, 454. [[CrossRef](#)]

8. Ferrara, L.; Van Mullem, T.; Alonso, M.C.; Antonaci, P.; Borg, R.P.; Cuenca, E.; Jefferson, A.; Ng, P.L.; Peled, A.; Roig-Flores, M.; et al. Experimental characterization of the self-healing capacity of cement based materials and its effects on the material performance: A state of the art report by COST Action SARCOS WG2. *Constr. Build. Mater.* **2018**, *167*, 115–142. [[CrossRef](#)]
9. Van Tittelboom, K.; De Belie, N. Self-healing in cementitious materials—A review. *Materials* **2013**, *6*, 2182–2217. [[CrossRef](#)]
10. Hearn, N. Self-sealing, autogenous healing and continued hydration: What is the difference? *Mater. Struct.* **1998**, *31*, 563. [[CrossRef](#)]
11. Koenders, E.; Ukrainczyk, N.; Caggiano, A. Modelling the Self-Healing Potential of Dissoluble Encapsulated Cement. In Proceedings of the 7th European Conference on Computational Fluid Dynamics (ECFD 7), Glasgow, UK, 11–15 June 2018.
12. Yang, S.; Caggiano, A.; Yi, M.; Ukrainczyk, N.; Koenders, E. Modelling autogenous self-healing with dissoluble encapsulated particles using a phase field approach. In *Conference: Mecánica Computacional, Santa Fe, Argentina, 5–7 Noviembre 2019*; Asociación Argentina de Mecánica Computacional: Santa Fe, Argentina, 2019; Volume 37, pp. 1457–1467.
13. Huang, H.; Ye, G.; Damidot, D. Effect of blast furnace slag on self-healing of microcracks in cementitious materials. *Cem. Concr. Res.* **2014**, *60*, 68–82. [[CrossRef](#)]
14. Jonkers, H.M. Self healing concrete: A biological approach. In *Self Healing Materials*; Springer: Berlin/Heidelberg, Germany, 2007; pp. 195–204.
15. Ghosh, S.K. *Self-Healing Materials: Fundamentals, Design Strategies, and Applications*; Wiley-vch: Weinheim, Germany, 2009.
16. De Rooij, M.; Van Tittelboom, K.; De Belie, N.; Schlangen, E. *Self-Healing Phenomena in Cement-Based Materials: State-of-the-Art Report of RILEM Technical Committee 221-SHC: Self-Healing Phenomena in Cement-Based Materials*; Springer: Berlin/Heidelberg, Germany, 2013; Volume 11.
17. Li, V.C.; Yang, E.H. Self healing in concrete materials. In *Self Healing Materials*; Springer: Berlin/Heidelberg, Germany, 2007; pp. 161–193.
18. Van Tittelboom, K.; Gruyaert, E.; Rahier, H.; De Belie, N. Influence of mix composition on the extent of autogenous crack healing by continued hydration or calcium carbonate formation. *Constr. Build. Mater.* **2012**, *37*, 349–359. [[CrossRef](#)]
19. Snoeck, D.; De Belie, N. Repeated autogenous healing in strain-hardening cementitious composites by using superabsorbent polymers. *J. Mater. Civ. Eng.* **2016**, *28*, 04015086. [[CrossRef](#)]
20. Snoeck, D.; De Belie, N. From straw in bricks to modern use of microfibers in cementitious composites for improved autogenous healing—A review. *Constr. Build. Mater.* **2015**, *95*, 774–787. [[CrossRef](#)]
21. Mihashi, H.; Nishiwaki, T. Development of engineered self-healing and self-repairing concrete-state-of-the-art report. *J. Adv. Concr. Technol.* **2012**, *10*, 170–184. [[CrossRef](#)]
22. Rule, J.D.; Brown, E.N.; Sottos, N.R.; White, S.R.; Moore, J.S. Wax-protected catalyst microspheres for efficient self-healing materials. *Adv. Mater.* **2005**, *17*, 205–208. [[CrossRef](#)]
23. Dong, B.; Ding, W.; Qin, S.; Han, N.; Fang, G.; Liu, Y.; Xing, F.; Hong, S. Chemical self-healing system with novel microcapsules for corrosion inhibition of rebar in concrete. *Cem. Concr. Compos.* **2018**, *85*, 83–91. [[CrossRef](#)]
24. Snoeck, D.; Van Tittelboom, K.; Steuperaert, S.; Dubruel, P.; De Belie, N. Self-healing cementitious materials by the combination of microfibres and superabsorbent polymers. *J. Intell. Mater. Syst. Struct.* **2014**, *25*, 13–24. [[CrossRef](#)]
25. Alghamri, R.; Kanellopoulos, A.; Litina, C.; Al-Tabbaa, A. Preparation and polymeric encapsulation of powder mineral pellets for self-healing cement based materials. *Constr. Build. Mater.* **2018**, *186*, 247–262. [[CrossRef](#)]
26. Roig-Flores, M.; Moscato, S.; Serna, P.; Ferrara, L. Self-healing capability of concrete with crystalline admixtures in different environments. *Constr. Build. Mater.* **2015**, *86*, 1–11. [[CrossRef](#)]
27. Roig-Flores, M.; Pirritano, F.; Serna, P.; Ferrara, L. Effect of crystalline admixtures on the self-healing capability of early-age concrete studied by means of permeability and crack closing tests. *Constr. Build. Mater.* **2016**, *114*, 447–457. [[CrossRef](#)]
28. Van Tittelboom, K.; De Belie, N.; De Muynck, W.; Verstraete, W. Use of bacteria to repair cracks in concrete. *Cem. Concr. Res.* **2010**, *40*, 157–166. [[CrossRef](#)]

29. Wang, J.; Soens, H.; Verstraete, W.; De Belie, N. Self-healing concrete by use of microencapsulated bacterial spores. *Cem. Concr. Res.* **2014**, *56*, 139–152. [[CrossRef](#)]
30. Tan, N.P.B.; Keung, L.H.; Choi, W.H.; Lam, W.C.; Leung, H.N. Silica-based self-healing microcapsules for self-repair in concrete. *J. Appl. Polym. Sci.* **2016**, *133*. [[CrossRef](#)]
31. Aliko-Benítez, A.; Doblaré, M.; Sanz-Herrera, J. Chemical-diffusive modeling of the self-healing behavior in concrete. *Int. J. Solids Struct.* **2015**, *69*, 392–402. [[CrossRef](#)]
32. Huang, H.; Ye, G. Simulation of self-healing by further hydration in cementitious materials. *Cem. Concr. Compos.* **2012**, *34*, 460–467. [[CrossRef](#)]
33. Ferrara, L.; Di Luzio, G.; Krelani, V. Experimental Assessment and Numerical Modeling of Self Healing Capacity of Cement Based Materials via Fracture Mechanics Concepts. In Proceedings of the 9th International Conference on Fracture Mechanics of Concrete and Concrete Structures (FraMCoS-9), Berkeley, CA, USA, 29 May–1 June 2016; pp. 1–12.
34. Di Luzio, G.; Ferrara, L.; Krelani, V. A numerical model for the self-healing capacity of cementitious composites. In Proceedings of the Computational Modelling of Concrete Structures, St. Anton am Arlberg, Austria, 24–27 March 2014.
35. Zemskov, S.V.; Jonkers, H.M.; Vermolen, F.J. Mathematical models to predict the critical conditions for bacterial self-healing of concrete. In Proceedings of the International Conference on Mathematical Modeling and Computational Physics, Stará Lesná, Slovakia, 4–8 July 2011; pp. 108–121.
36. Zemskov, S.V.; Jonkers, H.M.; Vermolen, F.J. A mathematical model for bacterial self-healing of cracks in concrete. *J. Intell. Mater. Syst. Struct.* **2014**, *25*, 4–12. [[CrossRef](#)]
37. Hilloulin, B.; Grondin, F.; Matallah, M.; Loukili, A. Modelling of autogenous healing in ultra high performance concrete. *Cem. Concr. Res.* **2014**, *61*, 64–70. [[CrossRef](#)]
38. Di Luzio, G.; Ferrara, L.; Krelani, V. Numerical modeling of mechanical regain due to self-healing in cement based composites. *Cem. Concr. Compos.* **2018**, *86*, 190–205. [[CrossRef](#)]
39. Mergheim, J.; Steinmann, P. Phenomenological modelling of self-healing polymers based on integrated healing agents. *Comput. Mech.* **2013**, *52*, 681–692. [[CrossRef](#)]
40. Darabi, M.K.; Al-Rub, R.K.A.; Little, D.N. A continuum damage mechanics framework for modeling micro-damage healing. *Int. J. Solids Struct.* **2012**, *49*, 492–513. [[CrossRef](#)]
41. Hilloulin, B.; Hilloulin, D.; Grondin, F.; Loukili, A.; De Belie, N. Mechanical regains due to self-healing in cementitious materials: Experimental measurements and micro-mechanical model. *Cem. Concr. Res.* **2016**, *80*, 21–32. [[CrossRef](#)]
42. Miao, S.; Wang, M.L.; Schreyer, H.L. Constitutive models for healing of materials with application to compaction of crushed rock salt. *J. Eng. Mech.* **1995**, *121*, 1122–1129. [[CrossRef](#)]
43. Barbero, E.J.; Greco, F.; Lonetti, P. Continuum damage-healing mechanics with application to self-healing composites. *Int. J. Damage Mech.* **2005**, *14*, 51–81. [[CrossRef](#)]
44. Barbero, E.J.; Ford, K.J. Characterization of self-healing fiber-reinforced polymer-matrix composite with distributed damage. *J. Adv. Mater. Covina* **2007**, *39*, 20–27.
45. Hazelwood, T.; Jefferson, A.D.; Lark, R.J.; Gardner, D.R. Numerical simulation of the long-term behaviour of a self-healing concrete beam vs standard reinforced concrete. *Eng. Struct.* **2015**, *102*, 176–188. [[CrossRef](#)]
46. Davies, R.; Jefferson, A. Micromechanical modelling of self-healing cementitious materials. *Int. J. Solids Struct.* **2017**, *113*, 180–191. [[CrossRef](#)]
47. Remmers, J.J.; de Borst, R. Numerical modelling of self healing mechanisms. In *Self Healing Materials*; Springer: Berlin/Heidelberg, Germany, 2007; pp. 365–380.
48. Alsheghri, A.A.; Al-Rub, R.K.A. Thermodynamic-based cohesive zone healing model for self-healing materials. *Mech. Res. Commun.* **2015**, *70*, 102–113. [[CrossRef](#)]
49. Alsheghri, A.A.; Al-Rub, R.K.A. Finite element implementation and application of a cohesive zone damage-healing model for self-healing materials. *Eng. Fract. Mech.* **2016**, *163*, 1–22. [[CrossRef](#)]
50. Zhang, Y.; Zhuang, X. A softening-healing law for self-healing quasi-brittle materials: Analyzing with strong discontinuity embedded approach. *Eng. Fract. Mech.* **2018**, *192*, 290–306. [[CrossRef](#)]
51. Gilabert, F.; Garoz, D.; Van Paepegem, W. Macro-and micro-modeling of crack propagation in encapsulation-based self-healing materials: Application of XFEM and cohesive surface techniques. *Mater. Des.* **2017**, *130*, 459–478. [[CrossRef](#)]

52. Zhou, S.; Zhu, H.; Yan, Z.; Ju, J.W.; Zhang, L. A micromechanical study of the breakage mechanism of microcapsules in concrete using PFC2D. *Constr. Build. Mater.* **2016**, *115*, 452–463. [[CrossRef](#)]
53. Caggiano, A.; Etse, G.; Ferrara, L.; Krelani, V. Zero-thickness interface constitutive theory for concrete self-healing effects. *Comput. Struct.* **2017**, *186*, 22–34. [[CrossRef](#)]
54. Steinbach, I. Phase-field models in materials science. *Model. Simul. Mater. Sci. Eng.* **2009**, *17*, 073001. [[CrossRef](#)]
55. Boettinger, W.J.; Warren, J.A.; Beckermann, C.; Karma, A. Phase-field simulation of solidification. *Annu. Rev. Mater. Res.* **2002**, *32*, 163–194. [[CrossRef](#)]
56. Chen, L.Q. Phase-field models for microstructure evolution. *Annu. Rev. Mater. Res.* **2002**, *32*, 113–140. [[CrossRef](#)]
57. Pan, S.; Zhu, M. A three-dimensional sharp interface model for the quantitative simulation of solutal dendritic growth. *Acta Mater.* **2010**, *58*, 340–352. [[CrossRef](#)]
58. Bangert, F.; Kuhl, D.; Meschke, G. Chemo-hygro-mechanical modelling and numerical simulation of concrete deterioration caused by alkali-silica reaction. *Int. J. Numer. Anal. Methods Geomech.* **2004**, *28*, 689–714. [[CrossRef](#)]
59. Wang, H.; Liu, F.; Zhai, H.; Wang, K. Application of the maximal entropy production principle to rapid solidification: A sharp interface model. *Acta Mater.* **2012**, *60*, 1444–1454. [[CrossRef](#)]
60. Ma, L.; Chen, R.; Yang, X.; Zhang, H. Numerical approximations for Allen-Cahn type phase field model of two-phase incompressible fluids with moving contact lines. *Commun. Comput. Phys.* **2017**, *21*, 867–889. [[CrossRef](#)]
61. Gómez, H.; Calo, V.M.; Bazilevs, Y.; Hughes, T.J. Isogeometric analysis of the Cahn–Hilliard phase-field model. *Comput. Methods Appl. Mech. Eng.* **2008**, *197*, 4333–4352. [[CrossRef](#)]
62. Talaiekhazan, A.; Keyvanfar, A.; Shafaghat, A.; Andalib, R.; Majid, M.; Fulazzaky, M.A.; Zin, R.M.; Lee, C.T.; Hussin, M.W.; Hamzah, N.; et al. A review of self-healing concrete research development. *J. Environ. Treat. Tech.* **2014**, *2*, 1–11.
63. Luhar, S.; Gourav, S. A review paper on self healing concrete. *J. Civ. Eng. Res.* **2015**, *5*, 53–58.
64. Yang, Y.; Yang, E.H.; Li, V.C. Autogenous healing of engineered cementitious composites at early age. *Cem. Concr. Res.* **2011**, *41*, 176–183. [[CrossRef](#)]
65. Edvardsen, C. Water permeability and autogenous healing of cracks in concrete. *Mater. J.* **1999**, *96*, 448–454.
66. Van Tittelboom, K.; De Belie, N.; Lehmann, F.; Grosse, C.U. Acoustic emission analysis for the quantification of autonomous crack healing in concrete. *Constr. Build. Mater.* **2012**, *28*, 333–341. [[CrossRef](#)]
67. De Belie, N.; Gruyaert, E.; Al-Tabbaa, A.; Antonaci, P.; Baera, C.; Bajare, D.; Darquennes, A.; Davies, R.; Ferrara, L.; Jefferson, T.; et al. A review of self-healing concrete for damage management of structures. *Adv. Mater. Interfaces* **2018**, *5*, 1800074. [[CrossRef](#)]
68. Ferrara, L.; Krelani, V.; Carsana, M. A “fracture testing” based approach to assess crack healing of concrete with and without crystalline admixtures. *Constr. Build. Mater.* **2014**, *68*, 535–551. [[CrossRef](#)]
69. Yang, Y.; Lepech, M.D.; Yang, E.H.; Li, V.C. Autogenous healing of engineered cementitious composites under wet–dry cycles. *Cem. Concr. Res.* **2009**, *39*, 382–390. [[CrossRef](#)]
70. Reinhardt, H.; Jonkers, H.; Van Tittelboom, K.; Snoeck, D.; De Belie, N.; De Muyneck, W.; Verstraete, W.; Wang, J.; Mechtcherine, V. Recovery against environmental action. In *Self-Healing Phenomena in Cement-Based Materials*; Springer: Berlin/Heidelberg, Germany, 2013; pp. 65–117.
71. Qureshi, T.; Kanellopoulos, A.; Al-Tabbaa, A. Autogenous self-healing of cement with expansive minerals-I: Impact in early age crack healing. *Constr. Build. Mater.* **2018**, *192*, 768–784. [[CrossRef](#)]
72. Clear, C. *The Effects of Autogenous Healing upon the Leakage of Water through Cracks in Concrete*; Tech Rpt. 559; Transport Research Laboratory: Crowthorne, UK, 1985.
73. Meichsner, H. Über die Selbstdichtung von Trennrissen in Beton. *Beton-Und Stahlbetonbau* **1992**, *87*, 95–99. [[CrossRef](#)]
74. Reinhardt, H.W.; Jooss, M. Permeability and self-healing of cracked concrete as a function of temperature and crack width. *CEment Concr. Res.* **2003**, *33*, 981–985. [[CrossRef](#)]
75. Neville, A. Autogenous healing—A concrete miracle? *Concr. Int.* **2002**, *24*, 76–82.
76. Huang, H.; Ye, G.; Damidot, D. Characterization and quantification of self-healing behaviors of microcracks due to further hydration in cement paste. *Cem. Concr. Res.* **2013**, *52*, 71–81. [[CrossRef](#)]

77. Jefferson, T.; Javierre, E.; Freeman, B.; Zaoui, A.; Koenders, E.; Ferrara, L. Research progress on numerical models for self-healing cementitious materials. *Adv. Mater. Interfaces* **2018**, *5*, 1701378. [[CrossRef](#)]
78. Lee, Y.S.; Ryou, J.S. Self healing behavior for crack closing of expansive agent via granulation/film coating method. *Constr. Build. Mater.* **2014**, *71*, 188–193. [[CrossRef](#)]
79. Ahn, T.H.; Kishi, T. Crack self-healing behavior of cementitious composites incorporating various mineral admixtures. *J. Adv. Concr. Technol.* **2010**, *8*, 171–186. [[CrossRef](#)]
80. Jonkers, H.M.; Thijssen, A.; Muyzer, G.; Copuroglu, O.; Schlangen, E. Application of bacteria as self-healing agent for the development of sustainable concrete. *Ecol. Eng.* **2010**, *36*, 230–235. [[CrossRef](#)]
81. Wiktor, V.; Jonkers, H.M. Quantification of crack-healing in novel bacteria-based self-healing concrete. *Cem. Concr. Compos.* **2011**, *33*, 763–770. [[CrossRef](#)]
82. Gupta, S.; Dai Pang, S.; Kua, H.W. Autonomous healing in concrete by bio-based healing agents—A review. *Constr. Build. Mater.* **2017**, *146*, 419–428. [[CrossRef](#)]
83. Jonkers, H.M. Bacteria-based self-healing concrete. *Heron* **2011**, *56*.
84. Wang, J.Y.; De Belie, N.; Verstraete, W. Diatomaceous earth as a protective vehicle for bacteria applied for self-healing concrete. *J. Ind. Microbiol. Biotechnol.* **2012**, *39*, 567–577. [[CrossRef](#)] [[PubMed](#)]
85. Wang, J.; Snoeck, D.; Van Vlierberghe, S.; Verstraete, W.; De Belie, N. Application of hydrogel encapsulated carbonate precipitating bacteria for approaching a realistic self-healing in concrete. *Constr. Build. Mater.* **2014**, *68*, 110–119. [[CrossRef](#)]
86. Luo, M.; Qian, C.X.; Li, R.Y. Factors affecting crack repairing capacity of bacteria-based self-healing concrete. *Constr. Build. Mater.* **2015**, *87*, 1–7. [[CrossRef](#)]
87. Wang, J.; Mignon, A.; Snoeck, D.; Wiktor, V.; Van Vlierberghe, S.; Boon, N.; De Belie, N. Application of modified-alginate encapsulated carbonate producing bacteria in concrete: A promising strategy for crack self-healing. *Front. Microbiol.* **2015**, *6*, 1088. [[CrossRef](#)]
88. Khaliq, W.; Ehsan, M.B. Crack healing in concrete using various bio influenced self-healing techniques. *Constr. Build. Mater.* **2016**, *102*, 349–357. [[CrossRef](#)]
89. Thao, T.D.P.; Johnson, T.J.S.; Tong, Q.S.; Dai, P.S. Implementation of self-healing in concrete—proof of concept. *IES J. Part A Civ. Struct. Eng.* **2009**, *2*, 116–125. [[CrossRef](#)]
90. Van Belleghem, B.; Kessler, S.; Van den Heede, P.; Van Tittelboom, K.; De Belie, N. Chloride induced reinforcement corrosion behavior in self-healing concrete with encapsulated polyurethane. *Cem. Concr. Res.* **2018**, *113*, 130–139. [[CrossRef](#)]
91. Jiang, Z.; Li, W.; Yuan, Z. Influence of mineral additives and environmental conditions on the self-healing capabilities of cementitious materials. *Cem. Concr. Compos.* **2015**, *57*, 116–127. [[CrossRef](#)]
92. Jaroenratanapirom, D.; Sahamitmongkol, R. Effects of different mineral additives and cracking ages on self-healing performance of mortar. In Proceedings of the 6th Annual Concrete Conference, Phetchaburi, Thailand, 20–23 October 2010; pp. 551–556.
93. Jiang, Z.; Li, W.; Yuan, Z.; Yang, Z. Self-healing of cracks in concrete with various crystalline mineral additives in underground environment. *J. Wuhan Univ. Technol.-Mater. Sci. Ed.* **2014**, *29*, 938–944. [[CrossRef](#)]
94. Kanellopoulos, A.; Qureshi, T.; Al-Tabbaa, A. Glass encapsulated minerals for self-healing in cement based composites. *Constr. Build. Mater.* **2015**, *98*, 780–791. [[CrossRef](#)]
95. Qureshi, T.; Kanellopoulos, A.; Al-Tabbaa, A. Encapsulation of expansive powder minerals within a concentric glass capsule system for self-healing concrete. *Constr. Build. Mater.* **2016**, *121*, 629–643. [[CrossRef](#)]
96. Sisomphon, K.; Copuroglu, O.; Koenders, E. Self-healing of surface cracks in mortars with expansive additive and crystalline additive. *Cem. Concr. Compos.* **2012**, *34*, 566–574. [[CrossRef](#)]
97. Ahn, T.; Kishi, T. The effect of geo-materials on the autogenous healing behavior of cracked concrete. In *Concrete Repair, Rehabilitation and Retrofitting II, Cape Town, South Africa*; CRC Press: Boca Raton, FL, USA, 2008; pp. 125–126.
98. Buller, A.S.; Lee, K.M.; Jang, S.Y. Mechanical recovery of cracked fiber-reinforced mortar incorporating crystalline admixture, expansive agent, and geomaterial. *Adv. Mater. Sci. Eng.* **2019**, *2019*, 3420349. [[CrossRef](#)]
99. Lucas, S.S.; Moxham, C.; Tziviloglou, E.; Jonkers, H. Study of self-healing properties in concrete with bacteria encapsulated in expanded clay. *Sci. Technol. Mater.* **2018**, *30*, 93–98. [[CrossRef](#)]

100. Jonkers, H.M.; Schlangen, E. A two component bacteria-based self-healing concrete. In Proceedings of the 2nd International Conference on Concrete Repair, Rehabilitation and Retrofitting, Cape Town, South Africa, 24–26 November 2008; pp. 119–120.
101. Jonkers, H.M.; Schlangen, E. Crack repair by concrete-immobilized bacteria. In Proceedings of the First International Conference on Self Healing Materials, Noordwijk Aan Zee, The Netherlands, 18–20 April 2007; Volume 18, p. 20.
102. Kua, H.W.; Gupta, S.; Aday, A.N.; Srubar III, W.V. Biochar-immobilized bacteria and superabsorbent polymers enable self-healing of fiber-reinforced concrete after multiple damage cycles. *Cem. Concr. Compos.* **2019**, *100*, 35–52. [[CrossRef](#)]
103. Wu, M.; Hu, X.; Zhang, Q.; Xue, D.; Zhao, Y. Growth environment optimization for inducing bacterial mineralization and its application in concrete healing. *Constr. Build. Mater.* **2019**, *209*, 631–643. [[CrossRef](#)]
104. Li, V.C.; Herbert, E. Robust self-healing concrete for sustainable infrastructure. *J. Adv. Concr. Technol.* **2012**, *10*, 207–218. [[CrossRef](#)]
105. Lee, Y.S.; Park, W. Current challenges and future directions for bacterial self-healing concrete. *Appl. Microbiol. Biotechnol.* **2018**, *102*, 3059–3070. [[CrossRef](#)]
106. Rao, M.; Reddy, V.S.; Hafsa, M.; Veena, P.; Anusha, P. Bioengineered concrete—a sustainable self-healing construction material. *Res. J. Eng. Sci. ISSN* **2013**, 2278, 9472.
107. Xu, J.; Yao, W. Multiscale mechanical quantification of self-healing concrete incorporating non-ureolytic bacteria-based healing agent. *Cem. Concr. Res.* **2014**, *64*, 1–10. [[CrossRef](#)]
108. Alazhari, M.; Sharma, T.; Heath, A.; Cooper, R.; Paine, K. Application of expanded perlite encapsulated bacteria and growth media for self-healing concrete. *Constr. Build. Mater.* **2018**, *160*, 610–619. [[CrossRef](#)]
109. Han, S.; Choi, E.K.; Park, W.; Yi, C.; Chung, N. Effectiveness of expanded clay as a bacteria carrier for self-healing concrete. *Appl. Biol. Chem.* **2019**, *62*, 19. [[CrossRef](#)]
110. Alghamri, R.; Kanellopoulos, A.; Al-Tabbaa, A. Impregnation and encapsulation of lightweight aggregates for self-healing concrete. *Constr. Build. Mater.* **2016**, *124*, 910–921. [[CrossRef](#)]
111. Seifan, M.; Samani, A.K.; Berenjian, A. Bioconcrete: Next generation of self-healing concrete. *Appl. Microbiol. Biotechnol.* **2016**, *100*, 2591–2602. [[CrossRef](#)] [[PubMed](#)]
112. Yang, Z.; Hollar, J.; He, X.; Shi, X. A self-healing cementitious composite using oil core/silica gel shell microcapsules. *Cem. Concr. Compos.* **2011**, *33*, 506–512. [[CrossRef](#)]
113. Dong, B.; Fang, G.; Ding, W.; Liu, Y.; Zhang, J.; Han, N.; Xing, F. Self-healing features in cementitious material with urea–formaldehyde/epoxy microcapsules. *Constr. Build. Mater.* **2016**, *106*, 608–617. [[CrossRef](#)]
114. Muhammad, N.Z.; Shafaghat, A.; Keyvanfar, A.; Majid, M.Z.A.; Ghoshal, S.; Yasouj, S.E.M.; Ganiyu, A.A.; Kouchaksaraei, M.S.; Kamyab, H.; Taheri, M.M.; et al. Tests and methods of evaluating the self-healing efficiency of concrete: A review. *Constr. Build. Mater.* **2016**, *112*, 1123–1132. [[CrossRef](#)]
115. Hu, Z.X.; Hu, X.M.; Cheng, W.M.; Zhao, Y.Y.; Wu, M.Y. Performance optimization of one-component polyurethane healing agent for self-healing concrete. *Constr. Build. Mater.* **2018**, *179*, 151–159. [[CrossRef](#)]
116. Dry, C.M. Design of self-growing, self-sensing, and self-repairing materials for engineering applications. In *Smart Materials and MEMS, Melbourne, Australia, 2000*; International Society for Optics and Photonics: Bellingham, WA, USA, 2001; Volume 4234, pp. 23–29.
117. Hilloulin, B.; Van Tittelboom, K.; Gruyaert, E.; De Belie, N.; Loukili, A. Design of polymeric capsules for self-healing concrete. *Cem. Concr. Compos.* **2015**, *55*, 298–307. [[CrossRef](#)]
118. Van Tittelboom, K.; Tsangouri, E.; Van Hemelrijck, D.; De Belie, N. The efficiency of self-healing concrete using alternative manufacturing procedures and more realistic crack patterns. *Cem. Concr. Compos.* **2015**, *57*, 142–152. [[CrossRef](#)]
119. Dry, C. Procedures developed for self-repair of polymer matrix composite materials. *Compos. Struct.* **1996**, *35*, 263–269. [[CrossRef](#)]
120. Pang, J.W.; Bond, I.P. A hollow fibre reinforced polymer composite encompassing self-healing and enhanced damage visibility. *Compos. Sci. Technol.* **2005**, *65*, 1791–1799. [[CrossRef](#)]
121. Zhu, Y.; Ye, X.J.; Rong, M.Z.; Zhang, M.Q. Self-healing glass fiber/epoxy composites with polypropylene tubes containing self-pressurized epoxy and mercaptan healing agents. *Compos. Sci. Technol.* **2016**, *135*, 146–152. [[CrossRef](#)]
122. Huang, M.; Zhang, H.; Yang, J. Synthesis of organic silane microcapsules for self-healing corrosion resistant polymer coatings. *Corrosion Sci.* **2012**, *65*, 561–566. [[CrossRef](#)]

123. Shen, J.; Yang, X.; Wang, Q. Mass and volume conservation in phase field models for binary fluids. *Commun. Comput. Phys.* **2013**, *13*, 1045–1065. [[CrossRef](#)]
124. Karma, A.; Rappel, W.J. Phase-field method for computationally efficient modeling of solidification with arbitrary interface kinetics. *Phys. Rev. E* **1996**, *53*, R3017. [[CrossRef](#)]
125. Flower, H.; Gregson, P. Solid state phase transformations in aluminium alloys containing lithium. *Mater. Sci. Technol.* **1987**, *3*, 81–90. [[CrossRef](#)]
126. Steinbach, I.; Apel, M. Multi phase field model for solid state transformation with elastic strain. *Phys. D Nonlinear Phenom.* **2006**, *217*, 153–160. [[CrossRef](#)]
127. Krill Iii, C.; Chen, L.Q. Computer simulation of 3-D grain growth using a phase-field model. *Acta Mater.* **2002**, *50*, 3059–3075. [[CrossRef](#)]
128. Moelans, N.; Blanpain, B.; Wollants, P. Quantitative analysis of grain boundary properties in a generalized phase field model for grain growth in anisotropic systems. *Phys. Rev. B* **2008**, *78*, 024113. [[CrossRef](#)]
129. Kazaryan, A.; Wang, Y.; Dregia, S.; Patton, B.R. Generalized phase-field model for computer simulation of grain growth in anisotropic systems. *Phys. Rev. B* **2000**, *61*, 14275. [[CrossRef](#)]
130. Zeng, Y.; Hunter, A.; Beyerlein, I.J.; Koslowski, M. A phase field dislocation dynamics model for a bicrystal interface system: An investigation into dislocation slip transmission across cube-on-cube interfaces. *Int. J. Plast.* **2016**, *79*, 293–313. [[CrossRef](#)]
131. Levitas, V.I.; Roy, A.M. Multiphase phase field theory for temperature-induced phase transformations: Formulation and application to interfacial phases. *Acta Mater.* **2016**, *105*, 244–257. [[CrossRef](#)]
132. Ravash, H.; Vanherpe, L.; Vleugels, J.; Moelans, N. Three-dimensional phase-field study of grain coarsening and grain shape accommodation in the final stage of liquid-phase sintering. *J. Eur. Ceram. Soc.* **2017**, *37*, 2265–2275. [[CrossRef](#)]
133. Deckelnick, K.; Elliott, C.M.; Styles, V. Double obstacle phase field approach to an inverse problem for a discontinuous diffusion coefficient. *Inverse Probl.* **2016**, *32*, 045008. [[CrossRef](#)]
134. Heinonen, V.; Achim, C.; Kosterlitz, J.; Ying, S.C.; Lowengrub, J.; Ala-Nissila, T. Consistent hydrodynamics for phase field crystals. *Phys. Rev. Lett.* **2016**, *116*, 024303. [[CrossRef](#)]
135. Wang, N.; Bevan, K.H.; Provatas, N. Phase-field-crystal model for electromigration in metal interconnects. *Phys. Rev. Lett.* **2016**, *117*, 155901. [[CrossRef](#)]
136. Miehe, C.; Hofacker, M.; Welschinger, F. A phase field model for rate-independent crack propagation: Robust algorithmic implementation based on operator splits. *Comput. Methods Appl. Mech. Eng.* **2010**, *199*, 2765–2778. [[CrossRef](#)]
137. Spatschek, R.; Brener, E.; Karma, A. Phase field modeling of crack propagation. *Philos. Mag.* **2011**, *91*, 75–95. [[CrossRef](#)]
138. Spatschek, R.; Hartmann, M.; Brener, E.; Müller-Krumbhaar, H.; Kassner, K. Phase field modeling of fast crack propagation. *Phys. Rev. Lett.* **2006**, *96*, 015502. [[CrossRef](#)]
139. Karma, A.; Lobkovsky, A.E. Unsteady crack motion and branching in a phase-field model of brittle fracture. *Phys. Rev. Lett.* **2004**, *92*, 245510. [[CrossRef](#)] [[PubMed](#)]
140. Henry, H.; Levine, H. Dynamic instabilities of fracture under biaxial strain using a phase field model. *Phys. Rev. Lett.* **2004**, *93*, 105504. [[CrossRef](#)] [[PubMed](#)]
141. Miehe, C.; Welschinger, F.; Hofacker, M. Thermodynamically consistent phase-field models of fracture: Variational principles and multi-field FE implementations. *Int. J. Numer. Methods Eng.* **2010**, *83*, 1273–1311. [[CrossRef](#)]
142. Chen, L.Q. Phase-field method of phase transitions/domain structures in ferroelectric thin films: A review. *J. Am. Ceram. Soc.* **2008**, *91*, 1835–1844. [[CrossRef](#)]
143. Gránásy, L.; Pusztai, T.; Börzsönyi, T.; Tóth, G.; Tegze, G.; Warren, J.; Douglas, J. Phase field theory of crystal nucleation and polycrystalline growth: A review. *J. Mater. Res.* **2006**, *21*, 309–319. [[CrossRef](#)]
144. Steinbach, I. Phase-field model for microstructure evolution at the mesoscopic scale. *Annu. Rev. Mater. Res.* **2013**, *43*, 89–107. [[CrossRef](#)]
145. Greenwood, M.; Provatas, N.; Rottler, J. Free energy functionals for efficient phase field crystal modeling of structural phase transformations. *Phys. Rev. Lett.* **2010**, *105*, 045702. [[CrossRef](#)]
146. Provatas, N.; Elder, K. *Phase-Field Methods in Materials Science and Engineering*; John Wiley & Sons: Weinheim, Germany, 2011.
147. Caginalp, G.; Fife, P. Phase-field methods for interfacial boundaries. *Phys. Rev. B* **1986**, *33*, 7792. [[CrossRef](#)]

148. Ginzburg, V.L.; Landau, L.D. On the theory of superconductivity. In *On Superconductivity and Superfluidity*; Springer: Berlin/Heidelberg, Germany, 2009; pp. 113–137.
149. Aldakheel, F. *Mechanics of Nonlocal Dissipative Solids: Gradient Plasticity and Phase Field Modeling of Ductile Fracture*; Institut für Mechanik (Bauwesen), Lehrstuhl I, Universität Stuttgart: Stuttgart, Germany, 2016. [[CrossRef](#)]
150. Aldakheel, F. A microscale model for concrete failure in poro-elasto-plastic media. *Theor. Appl. Fract. Mech.* **2020**, *107*, 102517. [[CrossRef](#)]
151. Cahn, J.W.; Hilliard, J.E. Free energy of a nonuniform system. I. Interfacial free energy. *J. Chem. Phys.* **1958**, *28*, 258–267. [[CrossRef](#)]
152. Allen, S.M.; Cahn, J.W. A microscopic theory for antiphase boundary motion and its application to antiphase domain coarsening. *Acta Metall.* **1979**, *27*, 1085–1095. [[CrossRef](#)]
153. Qin, R.; Bhadeshia, H. Phase field method. *Mater. Sci. Technol.* **2010**, *26*, 803–811. [[CrossRef](#)]
154. Karma, A.; Rappel, W.J. Quantitative phase-field modeling of dendritic growth in two and three dimensions. *Phys. Rev. E* **1998**, *57*, 4323. [[CrossRef](#)]
155. Steinbach, I.; Pezzolla, F.; Nestler, B.; Seeßelberg, M.; Prieler, R.; Schmitz, G.J.; Rezende, J.L. A phase field concept for multiphase systems. *Phys. D Nonlinear Phenom.* **1996**, *94*, 135–147. [[CrossRef](#)]
156. Karma, A.; Rappel, W.J. Phase-field model of dendritic sidebranching with thermal noise. *Phys. Rev. E* **1999**, *60*, 3614. [[CrossRef](#)]
157. Jafarzadeh, H.; Farrahi, G.H.; Javanbakht, M. Phase field modeling of crack growth with double-well potential including surface effects. *Contin. Mech. Thermodyn.* **2020**, *32*, 913–925. [[CrossRef](#)]
158. Hu, S.; Li, Y.; Zheng, Y.; Chen, L. Effect of solutes on dislocation motion—A phase-field simulation. *Int. J. Plast.* **2004**, *20*, 403–425. [[CrossRef](#)]
159. Koslowski, M.; Cuitino, A.M.; Ortiz, M. A phase-field theory of dislocation dynamics, strain hardening and hysteresis in ductile single crystals. *J. Mech. Phys. Solids* **2002**, *50*, 2597–2635. [[CrossRef](#)]
160. Yu, Y.M.; Liu, B.G.; Voigt, A. Phase-field modeling of anomalous spiral step growth on Si (001) surface. *Phys. Rev. B* **2009**, *79*, 235317. [[CrossRef](#)]
161. Caginalp, G.; Xie, W. Phase-field and sharp-interface alloy models. *Phys. Rev. E* **1993**, *48*, 1897. [[CrossRef](#)]
162. Collins, J.B.; Levine, H. Diffuse interface model of diffusion-limited crystal growth. *Phys. Rev. B* **1985**, *31*, 6119. [[CrossRef](#)] [[PubMed](#)]
163. Wheeler, A.A.; Murray, B.T.; Schaefer, R.J. Computation of dendrites using a phase field model. *Phys. D Nonlinear Phenom.* **1993**, *66*, 243–262. [[CrossRef](#)]
164. Wang, S.L.; Sekerka, R.F. Computation of the dendritic operating state at large supercoolings by the phase field model. *Phys. Rev. E* **1996**, *53*, 3760. [[CrossRef](#)] [[PubMed](#)]
165. Beckermann, C.; Diepers, H.J.; Steinbach, I.; Karma, A.; Tong, X. Modeling melt convection in phase-field simulations of solidification. *J. Comput. Phys.* **1999**, *154*, 468–496. [[CrossRef](#)]
166. Ma, X.; Shi, S.; Woo, C.; Chen, L. The phase field model for hydrogen diffusion and γ -hydride precipitation in zirconium under non-uniformly applied stress. *Mech. Mater.* **2006**, *38*, 3–10. [[CrossRef](#)]
167. Lai, Z.W. Theory of ordering dynamics for Cu₃Au. *Phys. Rev. B* **1990**, *41*, 9239. [[CrossRef](#)]
168. Rubin, G.; Khachatryan, A. Three-dimensional model of precipitation of ordered intermetallics. *Acta Mater.* **1999**, *47*, 1995–2002. [[CrossRef](#)]
169. Pongsaksawad, W.; Powell, A.C.; Dussault, D. Phase-field modeling of transport-limited electrolysis in solid and liquid states. *J. Electrochem. Soc.* **2007**, *154*, F122–F133. [[CrossRef](#)]
170. Takaki, T. A phase-field topology optimization model using a double-obstacle function. In *ECCOMAS 2012-European Congress on Computational Methods in Applied Sciences and Engineering*; e-Book Full Papers: Vienna, Austria, 2012; pp. 8761–8768.
171. Leo, P.H.; Johnson, W. Spinodal decomposition and coarsening of stressed thin films on compliant substrates. *Acta Mater.* **2001**, *49*, 1771–1787. [[CrossRef](#)]
172. Echebarria, B.; Folch, R.; Karma, A.; Plapp, M. Quantitative phase-field model of alloy solidification. *Phys. Rev. E* **2004**, *70*, 061604. [[CrossRef](#)]
173. Karma, A.; Kessler, D.A.; Levine, H. Phase-field model of mode III dynamic fracture. *Phys. Rev. Lett.* **2001**, *87*, 045501. [[CrossRef](#)] [[PubMed](#)]
174. Karma, A.; Rappel, W.J. Numerical simulation of three-dimensional dendritic growth. *Phys. Rev. Lett.* **1996**, *77*, 4050. [[CrossRef](#)] [[PubMed](#)]

175. Warren, J.A.; Kobayashi, R.; Lobkovsky, A.E.; Carter, W.C. Extending phase field models of solidification to polycrystalline materials. *Acta Mater.* **2003**, *51*, 6035–6058. [[CrossRef](#)]
176. Nestler, B.; Garcke, H.; Stinner, B. Multicomponent alloy solidification: Phase-field modeling and simulations. *Phys. Rev. E* **2005**, *71*, 041609. [[CrossRef](#)]
177. Chen, Q.; Ma, N.; Wu, K.; Wang, Y. Quantitative phase field modeling of diffusion-controlled precipitate growth and dissolution in Ti–Al–V. *Scr. Mater.* **2004**, *50*, 471–476. [[CrossRef](#)]
178. Wang, Y.; Chen, L.Q.; Khachatryan, A. Kinetics of strain-induced morphological transformation in cubic alloys with a miscibility gap. *Acta Metall. Mater.* **1993**, *41*, 279–296. [[CrossRef](#)]
179. Van Noorden, T.; Eck, C. Phase field approximation of a kinetic moving-boundary problem modelling dissolution and precipitation. *Interfaces Free. Boundaries* **2011**, *13*, 29–55. [[CrossRef](#)]
180. Xu, Z.; Meakin, P. Phase-field modeling of solute precipitation and dissolution. *J. Chem. Phys.* **2008**, *129*, 014705. [[CrossRef](#)]
181. Chen, L.Q.; Yang, W. Computer simulation of the domain dynamics of a quenched system with a large number of nonconserved order parameters: The grain-growth kinetics. *Phys. Rev. B* **1994**, *50*, 15752. [[CrossRef](#)]
182. Zhu, J.; Wang, T.; Ardell, A.; Zhou, S.; Liu, Z.; Chen, L. Three-dimensional phase-field simulations of coarsening kinetics of r particles in binary Ni–Al alloys. *Acta Mater.* **2004**, *52*, 2837–2845. [[CrossRef](#)]
183. Lowengrub, J.S.; Rätz, A.; Voigt, A. Phase-field modeling of the dynamics of multicomponent vesicles: Spinodal decomposition, coarsening, budding, and fission. *Phys. Rev. E* **2009**, *79*, 031926. [[CrossRef](#)] [[PubMed](#)]
184. Hu, S.; Chen, L. Solute segregation and coherent nucleation and growth near a dislocation—A phase-field model integrating defect and phase microstructures. *Acta Mater.* **2001**, *49*, 463–472. [[CrossRef](#)]
185. Rodney, D.; Le Bouar, Y.; Finel, A. Phase field methods and dislocations. *Acta Mater.* **2003**, *51*, 17–30. [[CrossRef](#)]
186. Kassner, K.; Misbah, C.; Müller, J.; Kappey, J.; Kohlert, P. Phase-field modeling of stress-induced instabilities. *Phys. Rev. E* **2001**, *63*, 036117. [[CrossRef](#)] [[PubMed](#)]
187. Kassner, K.; Misbah, C. A phase-field approach for stress-induced instabilities. *EPL (Europhys. Lett.)* **1999**, *46*, 217. [[CrossRef](#)]
188. Du, Q.; Liu, C.; Wang, X. Simulating the deformation of vesicle membranes under elastic bending energy in three dimensions. *J. Comput. Phys.* **2006**, *212*, 757–777. [[CrossRef](#)]
189. Biben, T.; Kassner, K.; Misbah, C. Phase-field approach to three-dimensional vesicle dynamics. *Phys. Rev. E* **2005**, *72*, 041921. [[CrossRef](#)]
190. Léonard, F.; Desai, R.C. Alloy decomposition and surface instabilities in thin films. *Phys. Rev. B* **1998**, *57*, 4805. [[CrossRef](#)]
191. Wen, Y.H.; Chen, L.Q.; Hawk, J.A. Phase-field modeling of corrosion kinetics under dual-oxidants. *Model. Simul. Mater. Sci. Eng.* **2012**, *20*, 035013. [[CrossRef](#)]
192. Shibuta, Y.; Okajima, Y.; Suzuki, T. A phase-field simulation of bridge formation process in a nanometer-scale switch. *Scr. Mater.* **2006**, *55*, 1095–1098. [[CrossRef](#)]
193. Shibuta, Y.; Okajima, Y.; Suzuki, T. Phase-field modeling for electrodeposition process. *Sci. Technol. Adv. Mater.* **2007**, *8*, 511. [[CrossRef](#)]
194. Han, B.; Van der Ven, A.; Morgan, D.; Ceder, G. Electrochemical modeling of intercalation processes with phase field models. *Electrochim. Acta* **2004**, *49*, 4691–4699. [[CrossRef](#)]
195. Guyer, J.E.; Boettinger, W.J.; Warren, J.A.; McFadden, G.B. Phase field modeling of electrochemistry. I. Equilibrium. *Phys. Rev. E* **2004**, *69*, 021603. [[CrossRef](#)] [[PubMed](#)]
196. Choudhury, A.; Nestler, B. Grand-potential formulation for multicomponent phase transformations combined with thin-interface asymptotics of the double-obstacle potential. *Phys. Rev. E* **2012**, *85*, 021602. [[CrossRef](#)]
197. Böttger, B.; Eiken, J.; Steinbach, I. Phase field simulation of equiaxed solidification in technical alloys. *Acta Mater.* **2006**, *54*, 2697–2704. [[CrossRef](#)]
198. Oono, Y.; Puri, S. Study of phase-separation dynamics by use of cell dynamical systems. I. Modeling. *Phys. Rev. A* **1988**, *38*, 434. [[CrossRef](#)]
199. Blowey, J.; Elliott, C. *A Phase-Field Model with Double Obstacle Potential*; Citeseer: Princeton, NJ, USA, 1994.

200. Bhate, D.N.; Kumar, A.; Bower, A.F. Diffuse interface model for electromigration and stress voiding. *J. Appl. Phys.* **2000**, *87*, 1712–1721. [[CrossRef](#)]
201. Barrett, J.W.; Garcke, H.; Nürnberg, R. A phase field model for the electromigration of intergranular voids. *Interfaces Free Boundaries* **2007**, *9*, 171–210. [[CrossRef](#)]
202. Wang, Y.; Jin, Y.; Cuitino, A.; Khachaturyan, A. Phase field microelasticity theory and modeling of multiple dislocation dynamics. *Appl. Phys. Lett.* **2001**, *78*, 2324–2326. [[CrossRef](#)]
203. Wang, Y.U.; Jin, Y.; Cuitino, A.; Khachaturyan, A. Nanoscale phase field microelasticity theory of dislocations: Model and 3D simulations. *Acta Mater.* **2001**, *49*, 1847–1857. [[CrossRef](#)]
204. Karma, A.; Plapp, M. Spiral surface growth without desorption. *Phys. Rev. Lett.* **1998**, *81*, 4444. [[CrossRef](#)]
205. Braun, R.; Cahn, J.; McFadden, G.; Rushmeier, H.; Wheeler, A. Theory of anisotropic growth rates in the ordering of an fcc alloy. *Acta Mater.* **1998**, *46*, 1–12. [[CrossRef](#)]
206. Wang, Y.; Banerjee, D.; Su, C.; Khachaturyan, A. Field kinetic model and computer simulation of precipitation of L12 ordered intermetallics from fcc solid solution. *Acta Mater.* **1998**, *46*, 2983–3001. [[CrossRef](#)]
207. Kobayashi, R. Modeling and numerical simulations of dendritic crystal growth. *Phys. D Nonlinear Phenom.* **1993**, *63*, 410–423. [[CrossRef](#)]
208. Wang, S.L.; Sekerka, R.; Wheeler, A.; Murray, B.; Coriell, S.; Braun, R.; McFadden, G. Thermodynamically-consistent phase-field models for solidification. *Phys. D Nonlinear Phenom.* **1993**, *69*, 189–200. [[CrossRef](#)]
209. Wang, Y.U. Computer modeling and simulation of solid-state sintering: A phase field approach. *Acta Mater.* **2006**, *54*, 953–961. [[CrossRef](#)]
210. Wang, Y.; Khachaturyan, A. Three-dimensional field model and computer modeling of martensitic transformations. *Acta Mater.* **1997**, *45*, 759–773. [[CrossRef](#)]
211. Münch, I.; Krauß, M. An enhanced finite element technique for diffuse phase transition. *Comput. Mech.* **2015**, *56*, 691–708. [[CrossRef](#)]
212. Assadi, H. Phase-field modelling of electro-deoxidation in molten salt. *Model. Simul. Mater. Sci. Eng.* **2006**, *14*, 963. [[CrossRef](#)]
213. Li, Y.; Hu, S.; Liu, Z.; Chen, L. Effect of substrate constraint on the stability and evolution of ferroelectric domain structures in thin films. *Acta Mater.* **2002**, *50*, 395–411. [[CrossRef](#)]
214. Li, Y.; Chen, L. Temperature-strain phase diagram for Ba TiO₃ thin films. *Appl. Phys. Lett.* **2006**, *88*, 072905. [[CrossRef](#)]
215. Xu, J.; Wang, X.; Wang, B. Biochemical process of ureolysis-based microbial CaCO₃ precipitation and its application in self-healing concrete. *Appl. Microbiol. Biotechnol.* **2018**, *102*, 3121–3132. [[CrossRef](#)] [[PubMed](#)]
216. Vijay, K.; Murmu, M.; Deo, S.V. Bacteria based self healing concrete—A review. *Constr. Build. Mater.* **2017**, *152*, 1008–1014. [[CrossRef](#)]
217. Quayum, M.S.; Zhuang, X.; Rabczuk, T. Computational model generation and RVE design of self-healing concrete. *Front. Struct. Civ. Eng.* **2015**, *9*, 383–396. [[CrossRef](#)]
218. Mersmann, A.; Angerhöfer, M.; Franke, J. Controlled precipitation. *Chem. Eng. Technol. Ind. Chem.-Plant Equip.-Process Eng.-Biotechnol.* **1994**, *17*, 1–9. [[CrossRef](#)]
219. Mauludin, L.M.; Oucif, C. Modeling of self-healing concrete: A review. *J. Appl. Comput. Mech.* **2019**, *5*, 526–539.
220. Xu, Z.; Huang, H.; Li, X.; Meakin, P. Phase field and level set methods for modeling solute precipitation and/or dissolution. *Comput. Phys. Commun.* **2012**, *183*, 15–19. [[CrossRef](#)]
221. Redeker, M.; Rohde, C.; Sorin Pop, I. Upscaling of a tri-phase phase-field model for precipitation in porous media. *IMA J. Appl. Math.* **2016**, *81*, 898–939. [[CrossRef](#)]
222. Rohde, C.; von Wolff, L. A Ternary Cahn-Hilliard Navier-Stokes Model for Two Phase Flow with Precipitation and Dissolution. *arXiv* **2019**, arXiv:1912.09181.
223. Xu, Z.; Meakin, P. A phase-field approach to no-slip boundary conditions in dissipative particle dynamics and other particle models for fluid flow in geometrically complex confined systems. *J. Chem. Phys.* **2009**, *130*, 234103. [[CrossRef](#)]
224. Lin, G.; Bao, J.; Xu, Z. A three-dimensional phase field model coupled with a lattice kinetics solver for modeling crystal growth in furnaces with accelerated crucible rotation and traveling magnetic field. *Comput. Fluids* **2014**, *103*, 204–214. [[CrossRef](#)]

225. Xu, Z.; Meakin, P. Phase-field modeling of two-dimensional solute precipitation/dissolution: Solid fingers and diffusion-limited precipitation. *J. Chem. Phys.* **2011**, *134*, 044137. [[CrossRef](#)] [[PubMed](#)]
226. Bringedal, C.; von Wolff, L.; Pop, I.S. Phase field modeling of precipitation and dissolution processes in porous media: Upscaling and numerical experiments. *Multiscale Model. Simul.* **2020**, *18*, 1076–1112. [[CrossRef](#)]
227. Schwarze, C.; Gupta, A.; Hickel, T.; Kamachali, R.D. Phase-field study of ripening and rearrangement of precipitates under chemomechanical coupling. *Phys. Rev. B* **2017**, *95*, 174101. [[CrossRef](#)]
228. Müller, S.; Wolverson, C.; Wang, L.W.; Zunger, A. Predicting the size-and temperature-dependent shapes of precipitates in Al–Zn alloys. *Acta Mater.* **2000**, *48*, 4007–4020. [[CrossRef](#)]
229. Shi, R.; Wang, Y. Variant selection during α precipitation in Ti–6Al–4V under the influence of local stress—A simulation study. *Acta Mater.* **2013**, *61*, 6006–6024. [[CrossRef](#)]
230. Silberberg, M. *Principles of General Chemistry*; McGraw-Hill Education: London, UK, 2012.
231. Willard, H.H. Separation by precipitation from homogeneous solution. *Anal. Chem.* **1950**, *22*, 1372–1374. [[CrossRef](#)]
232. Cartwright, P.; Newman, E.; Wilson, D. Precipitation from homogeneous solution: A review. *Analyst* **1967**, *92*, 663–679. [[CrossRef](#)]
233. Collings, E. *Physics of Solid Solution Strengthening*; Springer Science & Business Media: Berlin, Germany, 2012.
234. Lifshitz, I.M.; Slyozov, V.V. The kinetics of precipitation from supersaturated solid solutions. *J. Phys. Chem. Solids* **1961**, *19*, 35–50. [[CrossRef](#)]
235. Awan, I.Z.; Khan, A.Q. Precipitation from Solid Solutions. *J. Chem. Soc. Pak.* **2017**, *39*, 319–336.
236. Callister, W.D. *Fundamentals of Materials Science and Engineering*; Wiley: London, UK, 2000; Volume 471660817.
237. Hou, H.; Zhao, Y.; Zhao, Y. Simulation of the precipitation process of ordered intermetallic compounds in binary and ternary Ni–Al-based alloys by the phase-field model. *Mater. Sci. Eng. A* **2009**, *499*, 204–207. [[CrossRef](#)]
238. Wen, Y.; Lill, J.; Chen, S.; Simmons, J. A ternary phase-field model incorporating commercial CALPHAD software and its application to precipitation in superalloys. *Acta Mater.* **2010**, *58*, 875–885. [[CrossRef](#)]
239. Wittmann, F. Structure of concrete with respect to crack formation. *Fract. Mech. Concr.* **1983**, *43*, 6.
240. Mazars, J.; Pijaudier-Cabot, G. Continuum damage theory—Application to concrete. *J. Eng. Mech.* **1989**, *115*, 345–365. [[CrossRef](#)]
241. Schlangen, E.; Van Mier, J. Micromechanical analysis of fracture of concrete. *Int. J. Damage Mech.* **1992**, *1*, 435–454. [[CrossRef](#)]
242. Lemaitre, J.; Chaboche, J.L. *Mechanics of Solid Materials*; Cambridge University Press: Cambridge, UK, 1994.
243. Meschke, G.; Lackner, R.; Mang, H.A. An anisotropic elastoplastic-damage model for plain concrete. *Int. J. Numer. Methods Eng.* **1998**, *42*, 703–727. [[CrossRef](#)]
244. Wriggers, P.; Moftah, S. Mesoscale models for concrete: Homogenisation and damage behaviour. *Finite Elem. Anal. Des.* **2006**, *42*, 623–636. [[CrossRef](#)]
245. Kuna, M. *Numerische Beanspruchungsanalyse von Rissen*; Springer: Berlin, Germany, 2008; Volume 2.
246. Sobolev, K.; Shah, S. *Nanotechnology of Concrete: Recent Developments and Future Perspectives*; ACI: Farmington Hills, MI, USA, 2008.
247. Pedersen, R.; Simone, A.; Sluys, L. An analysis of dynamic fracture in concrete with a continuum visco-elastic visco-plastic damage model. *Eng. Fract. Mech.* **2008**, *75*, 3782–3805. [[CrossRef](#)]
248. Hain, M.; Wriggers, P. Numerical homogenization of hardened cement paste. *Comput. Mech.* **2008**, *42*, 197–212. [[CrossRef](#)]
249. Kim, S.M.; Al-Rub, R.K.A. Meso-scale computational modeling of the plastic-damage response of cementitious composites. *Cem. Concr. Res.* **2011**, *41*, 339–358. [[CrossRef](#)]
250. Unger, J.F.; Eckardt, S.; Kooenke, C. A mesoscale model for concrete to simulate mechanical failure. *Comput. Concr.* **2011**, *8*, 401–423. [[CrossRef](#)]
251. Lohaus, L.; Oneschkow, N.; Wefer, M. Design model for the fatigue behaviour of normal-strength, high-strength and ultra-high-strength concrete. *Struct. Concr.* **2012**, *13*, 182–192. [[CrossRef](#)]
252. Anderson, T.L. *Fracture Mechanics: Fundamentals and Applications*; CRC Press: Boca Raton, FL, USA, 2017.
253. Zreid, I.; Kaliske, M. A gradient enhanced plasticity–damage microplane model for concrete. *Comput. Mech.* **2018**, *62*, 1239–1257. [[CrossRef](#)]

254. Schäfer, N.; Gudžulić, V.; Timothy, J.J.; Breitenbücher, R.; Meschke, G. Fatigue behavior of HPC and FRC under cyclic tensile loading: Experiments and modeling. *Struct. Concr.* **2019**, *20*, 1265–1278. [[CrossRef](#)]
255. Gebuhr, G.; Pise, M.; Sarhil, M.; Anders, S.; Brands, D.; Schröder, J. Analysis and evaluation of the pull-out behavior of hooked steel fibers embedded in high and ultra-high performance concrete for calibration of numerical models. *Struct. Concr.* **2019**, *20*, 1254–1264. [[CrossRef](#)]
256. Moës, N.; Belytschko, T. Extended finite element method for cohesive crack growth. *Eng. Fract. Mech.* **2002**, *69*, 813–833. [[CrossRef](#)]
257. Loehnert, S.; Mueller-Hoeppe, D.; Wriggers, P. 3D corrected XFEM approach and extension to finite deformation theory. *Int. J. Numer. Methods Eng.* **2011**, *86*, 431–452. [[CrossRef](#)]
258. Bourdin, B.; Francfort, G.A.; Marigo, J.J. The variational approach to fracture. *J. Elast.* **2008**, *91*, 5–148. [[CrossRef](#)]
259. Kuhn, C.; Müller, R. A continuum phase field model for fracture. *Eng. Fract. Mech.* **2010**, *77*, 3625–3634. [[CrossRef](#)]
260. Borden, M.J.; Verhoosel, C.V.; Scott, M.A.; Hughes, T.J.; Landis, C.M. A phase-field description of dynamic brittle fracture. *Comput. Methods Appl. Mech. Eng.* **2012**, *217*, 77–95. [[CrossRef](#)]
261. Hesch, C.; Weinberg, K. Thermodynamically consistent algorithms for a finite-deformation phase-field approach to fracture. *Int. J. Numer. Methods Eng.* **2014**, *99*, 906–924. [[CrossRef](#)]
262. Miehe, C.; Schanzel, L.M.; Ulmer, H. Phase field modeling of fracture in multi-physics problems. Part I. Balance of crack surface and failure criteria for brittle crack propagation in thermo-elastic solids. *Comput. Methods Appl. Mech. Eng.* **2015**, *294*, 449–485. [[CrossRef](#)]
263. Heister, T.; Wheeler, M.F.; Wick, T. A primal-dual active set method and predictor-corrector mesh adaptivity for computing fracture propagation using a phase-field approach. *Comput. Methods Appl. Mech. Eng.* **2015**, *290*, 466–495. [[CrossRef](#)]
264. Heider, Y.; Markert, B. A phase-field modeling approach of hydraulic fracture in saturated porous media. *Mech. Res. Commun.* **2017**, *80*, 38–46. [[CrossRef](#)]
265. Paggi, M.; Reinoso, J. Revisiting the problem of a crack impinging on an interface: A modeling framework for the interaction between the phase field approach for brittle fracture and the interface cohesive zone model. *Comput. Methods Appl. Mech. Eng.* **2017**, *321*, 145–172. [[CrossRef](#)]
266. Pillai, U.; Heider, Y.; Markert, B. A diffusive dynamic brittle fracture model for heterogeneous solids and porous materials with implementation using a user-element subroutine. *Comput. Mater. Sci.* **2018**, *153*, 36–47. [[CrossRef](#)]
267. Aldakheel, F.; Hudobivnik, B.; Hussein, A.; Wriggers, P. Phase-field modeling of brittle fracture using an efficient virtual element scheme. *Comput. Methods Appl. Mech. Eng.* **2018**, *341*, 443–466. [[CrossRef](#)]
268. Seleš, K.; Jurčević, A.; Tonković, Z.; Sorić, J. Crack propagation prediction in heterogeneous microstructure using an efficient phase-field algorithm. *Theor. Appl. Fract. Mech.* **2019**, *100*, 289–297. [[CrossRef](#)]
269. Nohi, N.; Aldakheel, F.; Wick, T.; Wriggers, P. An adaptive global-local approach for phase-field modeling of anisotropic brittle fracture. *Comput. Methods Appl. Mech. Eng.* **2020**, *361*, 112744. [[CrossRef](#)]
270. Heider, Y.; Sun, W. A phase field framework for capillary-induced fracture in unsaturated porous media: Drying-induced vs. hydraulic cracking. *Comput. Methods Appl. Mech. Eng.* **2020**, *359*, 112647. [[CrossRef](#)]
271. Aldakheel, F.; Tomann, C.; Lohaus, L.; Wriggers, P. Water-induced failure mechanics for concrete. *PAMM* **2019**, *19*, e201900140. [[CrossRef](#)]
272. Miehe, C.; Dal, H.; Schanzel, L.M.; Raina, A. A phase-field model for chemo-mechanical induced fracture in lithium-ion battery electrode particles. *Int. J. Numer. Methods Eng.* **2016**, *106*, 683–711. [[CrossRef](#)]
273. Ambati, M.; Gerasimov, T.; De Lorenzis, L. A review on phase-field models of brittle fracture and a new fast hybrid formulation. *Comput. Mech.* **2015**, *55*, 383–405. [[CrossRef](#)]
274. Tomann, C.; Lohaus, L.; Aldakheel, F.; Wriggers, P. Influence of water-induced damage mechanisms on the fatigue deterioration of high-strength concrete. In Proceedings of the 6th International Fib Congress: Concrete-Innovations in Materials, Design and Structures, Kraków, Poland, 27–29 May 2019.
275. Carollo, V.; Paggi, M.; Reinoso, J. The steady-state Archard adhesive wear problem revisited based on the phase field approach to fracture. *Int. J. Fract.* **2019**, *215*, 39–48. [[CrossRef](#)]
276. Steinke, C.; Kaliske, M. A phase-field crack model based on directional stress decomposition. *Comput. Mech.* **2019**, *63*, 1019–1046. [[CrossRef](#)]

277. Carrara, P.; Ambati, M.; Alessi, R.; De Lorenzis, L. A framework to model the fatigue behavior of brittle materials based on a variational phase-field approach. *Comput. Methods Appl. Mech. Eng.* **2020**, *361*, 112731. [[CrossRef](#)]
278. Heider, Y.; Reiche, S.; Siebert, P.; Markert, B. Modeling of hydraulic fracturing using a porous-media phase-field approach with reference to experimental data. *Eng. Fract. Mech.* **2018**, *202*, 116–134. [[CrossRef](#)]
279. Fantoni, F.; Bacigalupo, A.; Paggi, M.; Reinoso, J. A phase field approach for damage propagation in periodic microstructured materials. *Int. J. Fract.* **2019**, *223*, 53–76. [[CrossRef](#)]
280. Aldakheel, F.; Noh, N.; Wick, T.; Wriggers, P. A global-local approach for hydraulic phase-field fracture in poroelastic media. *Comput. Math. Appl.* **2020**. [[CrossRef](#)]
281. Yin, B.; Kaliske, M. An anisotropic phase-field model based on the equivalent crack surface energy density at finite strain. *Comput. Methods Appl. Mech. Eng.* **2020**, *369*, 113202. [[CrossRef](#)]
282. Khodadadian, A.; Noh, N.; Parvizi, M.; Abbaszadeh, M.; Wick, T.; Heitzinger, C. A Bayesian estimation method for variational phase-field fracture problems. *Comput. Mech.* **2020**, *66*, 827–849. [[CrossRef](#)] [[PubMed](#)]
283. Teichtmeister, S.; Kienle, D.; Aldakheel, F.; Keip, M.A. Phase field modeling of fracture in anisotropic brittle solids. *Int. J. Non-Linear Mech.* **2017**, *97*, 1–21. [[CrossRef](#)]
284. Bilgen, C.; Homberger, S.; Weinberg, K. Phase-field fracture simulations of the Brazilian splitting test. *Int. J. Fract.* **2019**, *220*, 85–98. [[CrossRef](#)]
285. Makvandi, R.; Duczek, S.; Juhre, D. A phase-field fracture model based on strain gradient elasticity. *Eng. Fract. Mech.* **2019**, *220*, 106648. [[CrossRef](#)]
286. Wriggers, P.; Aldakheel, F.; Lohaus, L.; Heist, M. Water-induced damage mechanisms of cyclically loaded High-performance concretes. *Bauingenieur* **2020**, *95*, 126–132.
287. Denli, F.A.; Gültekin, O.; Holzapfel, G.A.; Dal, H. A phase-field model for fracture of unidirectional fiber-reinforced polymer matrix composites. *Comput. Mech.* **2020**, *65*, 1149–1166. [[CrossRef](#)]
288. Schreiber, C.; Kuhn, C.; Müller, R.; Zohdi, T. A phase field modeling approach of cyclic fatigue crack growth. *Int. J. Fract.* **2020**, *225*, 89–100.
289. Zhuang, X.; Zhou, S.; Sheng, M.; Li, G. On the hydraulic fracturing in naturally-layered porous media using the phase field method. *Eng. Geol.* **2020**, *266*, 105306. [[CrossRef](#)]
290. Dittmann, M.; Krüger, M.; Schmidt, F.; Schuß, S.; Hesch, C. Variational modeling of thermomechanical fracture and anisotropic frictional mortar contact problems with adhesion. *Comput. Mech.* **2019**, *63*, 571–591. [[CrossRef](#)]
291. Hussein, A.; Wriggers, P.; Hudobivnik, B.; Aldakheel, F.; Guidault, P.A.; Allix, O. Treatment of Brittle Fracture in Solids with the Virtual Element Method. In *Virtual Design and Validation*; Springer: Berlin/Heidelberg, Germany, 2020; pp. 201–228.
292. Wick, T. *Multiphysics Phase-Field Fracture: Modeling, Adaptive Discretizations, and Solvers*; Walter de Gruyter GmbH & Co KG: Berlin, Germany, 2020; p. 28.
293. Geelen, R.; Plews, J.; Tupek, M.; Dolbow, J. An extended/generalized phase-field finite element method for crack growth with global-local enrichment. *Int. J. Numer. Methods Eng.* **2020**, *121*, 2534–2557. [[CrossRef](#)]
294. Ma, R.; Sun, W. FFT-based solver for higher-order and multi-phase-field fracture models applied to strongly anisotropic brittle materials. *Comput. Methods Appl. Mech. Eng.* **2020**, *362*, 112781. [[CrossRef](#)]
295. Tarafder, P.; Dan, S.; Ghosh, S. Finite deformation cohesive zone phase field model for crack propagation in multi-phase microstructures. *Comput. Mech.* **2020**, *66*, 723–743. [[CrossRef](#)]
296. De Lorenzis, L.; Gerasimov, T. Numerical Implementation of Phase-Field Models of Brittle Fracture. In *Modeling in Engineering Using Innovative Numerical Methods for Solids and Fluids*; Springer: Berlin/Heidelberg, Germany, 2020; pp. 75–101.
297. Miehe, C.; Hofacker, M.; Schänzel, L.M.; Aldakheel, F. Phase field modeling of fracture in multi-physics problems. Part II. Coupled brittle-to-ductile failure criteria and crack propagation in thermo-elastic-plastic solids. *Comput. Methods Appl. Mech. Eng.* **2015**, *294*, 486–522. [[CrossRef](#)]
298. Li, P.; Yvonnet, J.; Combescure, C. An extension of the phase field method to model interactions between interfacial damage and brittle fracture in elastoplastic composites. *Int. J. Mech. Sci.* **2020**, *179*, 105633. [[CrossRef](#)]
299. Ambati, M.; Kruse, R.; De Lorenzis, L. A phase-field model for ductile fracture at finite strains and its experimental verification. *Comput. Mech.* **2016**, *57*, 149–167. [[CrossRef](#)]

300. Barfusz, O.; Brepols, T.; van der Velden, T.; Frischkorn, J.; Reese, S. A single Gauss point continuum finite element formulation for gradient-extended damage at large deformations. *Comput. Methods Appl. Mech. Eng.* **2021**, *373*, 113440. [[CrossRef](#)]
301. Diehl, M.; Wicke, M.; Shanthraj, P.; Roters, F.; Brueckner-Foit, A.; Raabe, D. Coupled crystal plasticity–phase field fracture simulation study on damage evolution around a void: Pore shape versus crystallographic orientation. *JOM* **2017**, *69*, 872–878. [[CrossRef](#)]
302. Miehe, C.; Aldakheel, F.; Teichtmeister, S. Phase-field modeling of ductile fracture at finite strains: A robust variational-based numerical implementation of a gradient-extended theory by micromorphic regularization. *Int. J. Numer. Methods Eng.* **2017**, *111*, 816–863. [[CrossRef](#)]
303. Borden, M.J.; Hughes, T.J.; Landis, C.M.; Anvari, A.; Lee, I.J. A phase-field formulation for fracture in ductile materials: Finite deformation balance law derivation, plastic degradation, and stress triaxiality effects. *Comput. Methods Appl. Mech. Eng.* **2016**, *312*, 130–166. [[CrossRef](#)]
304. Miehe, C.; Aldakheel, F.; Raina, A. Phase field modeling of ductile fracture at finite strains: A variational gradient-extended plasticity-damage theory. *Int. J. Plast.* **2016**, *84*, 1–32. [[CrossRef](#)]
305. Alessi, R.; Marigo, J.J.; Maurini, C.; Vidoli, S. Coupling damage and plasticity for a phase-field regularisation of brittle, cohesive and ductile fracture: One-dimensional examples. *Int. J. Mech. Sci.* **2018**, *149*, 559–576. [[CrossRef](#)]
306. Aldakheel, F.; Mauthe, S.; Miehe, C. Towards Phase Field Modeling of Ductile Fracture in Gradient-Extended Elastic-Plastic Solids. *PAMM* **2014**, *14*, 411–412. [[CrossRef](#)]
307. Badnava, H.; Etemadi, E.; Msekh, M.A. A phase field model for rate-dependent ductile fracture. *Metals* **2017**, *7*, 180. [[CrossRef](#)]
308. Dittmann, M.; Aldakheel, F.; Schulte, J.; Schmidt, F.; Krüger, M.; Wriggers, P.; Hesch, C. Phase-field modeling of porous-ductile fracture in non-linear thermo-elasto-plastic solids. *Comput. Methods Appl. Mech. Eng.* **2020**, *361*, 112730. [[CrossRef](#)]
309. Choo, J.; Sun, W. Coupled phase-field and plasticity modeling of geological materials: From brittle fracture to ductile flow. *Comput. Methods Appl. Mech. Eng.* **2018**, *330*, 1–32. [[CrossRef](#)]
310. Seiler, M.; Linse, T.; Hantschke, P.; Kästner, M. An efficient phase-field model for fatigue fracture in ductile materials. *Eng. Fract. Mech.* **2020**, *224*, 106807. [[CrossRef](#)]
311. Dittmann, M.; Aldakheel, F.; Schulte, J.; Wriggers, P.; Hesch, C. Variational phase-field formulation of non-linear ductile fracture. *Comput. Methods Appl. Mech. Eng.* **2018**, *342*, 71–94. [[CrossRef](#)]
312. Yin, B.; Kaliske, M. A ductile phase-field model based on degrading the fracture toughness: Theory and implementation at small strain. *Comput. Methods Appl. Mech. Eng.* **2020**, *366*, 113068. [[CrossRef](#)]
313. Aldakheel, F.; Hudobivnik, B.; Wriggers, P. Virtual element formulation for phase-field modeling of ductile fracture. *Int. J. Multiscale Comput. Eng.* **2019**, *17*, 181–200. [[CrossRef](#)]
314. Kuhn, C.; Noll, T.; Müller, R. On phase field modeling of ductile fracture. *GAMM-Mitteilungen* **2016**, *39*, 35–54. [[CrossRef](#)]
315. Miehe, C.; Kienle, D.; Aldakheel, F.; Teichtmeister, S. Phase field modeling of fracture in porous plasticity: A variational gradient-extended Eulerian framework for the macroscopic analysis of ductile failure. *Comput. Methods Appl. Mech. Eng.* **2016**, *312*, 3–50. [[CrossRef](#)]
316. Fang, J.; Wu, C.; Li, J.; Liu, Q.; Wu, C.; Sun, G.; Li, Q. Phase field fracture in elasto-plastic solids: Variational formulation for multi-surface plasticity and effects of plastic yield surfaces and hardening. *Int. J. Mech. Sci.* **2019**, *156*, 382–396. [[CrossRef](#)]
317. Krüger, M.; Dittmann, M.; Aldakheel, F.; Härtel, A.; Wriggers, P.; Hesch, C. Porous-ductile fracture in thermo-elasto-plastic solids with contact applications. *Comput. Mech.* **2019**, 1–26. [[CrossRef](#)]
318. Nguyen, L.H.; Schilling, D. The multiscale finite element method for nonlinear continuum localization problems at full fine-scale fidelity, illustrated through phase-field fracture and plasticity. *J. Comput. Phys.* **2019**, *396*, 129–160. [[CrossRef](#)]
319. Azinpour, E.; Sa, J.C.D.; Santos, A.D.D. Micromechanically-motivated phase field approach to ductile fracture. *Int. J. Damage Mech.* **2020**. [[CrossRef](#)]
320. Aldakheel, F.; Wriggers, P.; Miehe, C. A modified Gurson-type plasticity model at finite strains: Formulation, numerical analysis and phase-field coupling. *Comput. Mech.* **2018**, *62*, 815–833. [[CrossRef](#)]
321. Brepols, T.; Wulfinghoff, S.; Reese, S. A gradient-extended two-surface damage-plasticity model for large deformations. *Int. J. Plast.* **2020**, *129*, 102635. [[CrossRef](#)]

322. Dean, A.; Reinoso, J.; Jha, N.; Mahdi, E.; Rolfes, R. A phase field approach for ductile fracture of short fibre reinforced composites. *Theor. Appl. Fract. Mech.* **2020**, 102495. [[CrossRef](#)]
323. Kienle, D.; Aldakheel, F.; Keip, M.A. A finite-strain phase-field approach to ductile failure of frictional materials. *Int. J. Solids Struct.* **2019**, 172, 147–162. [[CrossRef](#)]
324. Amin, W.; Ali, M.A.; Vajragupta, N.; Hartmaier, A. Studying grain boundary strengthening by dislocation-based strain gradient crystal plasticity coupled with a multi-phase-field model. *Materials* **2019**, 12, 2977. [[CrossRef](#)]
325. Wolf, E. Fatigue crack closure under cyclic tension. *Eng. Fract. Mech.* **1970**, 2, 37–45. [[CrossRef](#)]
326. Elber, W. The significance of fatigue crack closure. In *Damage Tolerance in Aircraft Structures*; ASTM International: West Conshohocken, PA, USA, 1971.
327. Vasudeven, A.; Sadananda, K.; Louat, N. A review of crack closure, fatigue crack threshold and related phenomena. *Mater. Sci. Eng. A* **1994**, 188, 1–22. [[CrossRef](#)]
328. Krueger, R. Virtual crack closure technique: History, approach, and applications. *Appl. Mech. Rev.* **2004**, 57, 109–143. [[CrossRef](#)]
329. Pippin, R.; Hohenwarter, A. Fatigue crack closure: A review of the physical phenomena. *Fatigue Fract. Eng. Mater. Struct.* **2017**, 40, 471–495. [[CrossRef](#)] [[PubMed](#)]
330. Aldakheel, F.; Hudobivnik, B.; Artioli, E.; Beirao da Veiga, L.; Wriggers, P. Curvilinear Virtual Elements for Contact Mechanics. *Comput. Methods Appl. Mech. Eng.* **2020**, accepted.
331. Francfort, G.A.; Marigo, J.J. Revisiting brittle fracture as an energy minimization problem. *J. Mech. Phys. Solids* **1998**, 46, 1319–1342. [[CrossRef](#)]
332. Mumford, D.B.; Shah, J. Optimal approximations by piecewise smooth functions and associated variational problems. *Commun. Pure Appl. Math.* **1989**, 42, 577–685. [[CrossRef](#)]

Publisher's Note: MDPI stays neutral with regard to jurisdictional claims in published maps and institutional affiliations.



© 2020 by the authors. Licensee MDPI, Basel, Switzerland. This article is an open access article distributed under the terms and conditions of the Creative Commons Attribution (CC BY) license (<http://creativecommons.org/licenses/by/4.0/>).